

Immunometabolic Effect of Nitric Oxide on Human Macrophages Challenged With the SARS-CoV2-Induced Cytokine Storm. A Fluxomic Approach

Sergio Sánchez-García,* Adrián Povo-Retana, Silvia Marin, Sergio Madurga, Marco Fariñas, Nuria Aleixandre, Antonio Castrillo, Juan V. de la Rosa, Carlota Alvarez-Lucena, Rodrigo Landauro-Vera, Patricia Prieto, Marta Cascante,* and Lisardo Boscá*

The cytokine storm associated with SARS-CoV-2 infection is one of the most distinctive pathological signatures in COVID-19 patients. Macrophages respond to this pro-inflammatory challenge by reprogramming their functional and metabolic phenotypes. Interestingly, human macrophages fail to express the inducible form of the NO synthase (NOS2) in response to pro-inflammatory activation and, therefore, NO is not synthesized by these cells. The contribution of exogenously added NO, via a chemical NO-donor, on the immunometabolic changes associated with the cytokine storm is investigated. By using metabolic, transcriptomic, and functional assays the effect of NO in human macrophages is evaluated and found specific responses. Moreover, through integrative fluxomic analysis, pathways modified by NO that contribute to the expression of a particular phenotype in human macrophages are identified, which includes a decrease in mitochondrial respiration and TCA with a slight increase in the glycolytic flux. A significant ROS increase and preserved cell viability are observed in the presence of NO, which may ease the inflammatory response and host defense. Also, NO reverses the cytokine storm-induced itaconate accumulation. These changes offer additional clues to understanding the potential crosstalk between NO and the COVID-19 cytokine storm-dependent signaling pathways.

1. Introduction

The infection by the Severe Acute Respiratory Syndrome Coronavirus 2 (SARS-CoV-2), and the subsequent acute respiratory disease (coronavirus disease 2019; COVID-19) generated a pandemic at the end of 2019 and constituted the first major health challenge of the 21st century,^[1] This pandemic resulted in a massive toll of disease and economic havoc, being responsible for more than 700 million reported cases and more than 7 million deaths (WHO). Nowadays, COVID-19 disease is still highly relevant, with more than 40 000 confirmed cases per month worldwide in March 2024. Furthermore, the prevalence of long-COVID in patients 3 months after infection is $\approx 10\%$ – 20% , according to the WHO (<https://www.who.int/europe/news-room/fact-sheets/item/post-covid-19-condition>), and 6.9% of US adults experienced symptoms in 2022 (<https://stacks.cdc.gov/view/cdc/132417>). This remains an unresolved issue, with a lack of specific and effective treatments. The

S. Sánchez-García, A. Povo-Retana, A. Castrillo, C. Alvarez-Lucena, R. Landauro-Vera, P. Prieto, L. Boscá
Instituto de Investigaciones Biomédicas Sols-Morreale, Consejo Superior de Investigaciones Científicas-Universidad Autónoma de Madrid
Arturo Duperier 4
Madrid 28029, Spain
E-mail: sgarcia@iib.uam.es; lbosca@iib.uam.es

S. Sánchez-García, A. Povo-Retana, A. Castrillo, C. Alvarez-Lucena, R. Landauro-Vera, P. Prieto, L. Boscá
Centro de Investigación Biomédica en Red de Enfermedades Cardiovasculares (CIBERCV)
Av. Monforte de Lemos 3–5, P-11, Madrid 28029, Spain
S. Marin, M. Fariñas, N. Aleixandre, M. Cascante
Department of Biochemistry and Molecular Biomedicine-Institute of Biomedicine (IBUB), Faculty of Biology
Universitat de Barcelona
Barcelona 08028, Spain
E-mail: martacascante@ub.edu
S. Marin, M. Cascante
Centro de Investigación Biomédica en Red de Enfermedades Hepáticas y Digestivas (CIBEREHD)
Av. Monforte de Lemos 3–5, P-11, Madrid 28029, Spain

 The ORCID identification number(s) for the author(s) of this article can be found under <https://doi.org/10.1002/adhm.202401688>

© 2024 The Author(s). Advanced Healthcare Materials published by Wiley-VCH GmbH. This is an open access article under the terms of the [Creative Commons Attribution-NonCommercial](https://creativecommons.org/licenses/by-nc/4.0/) License, which permits use, distribution and reproduction in any medium, provided the original work is properly cited and is not used for commercial purposes.

DOI: 10.1002/adhm.202401688

COVID-19 trait emphasized the relevance of identifying the physiopathological mechanisms involved and their translation into therapeutic and health interventions. In this regard, the diversity in the interactions between the SARS-CoV-2 and the patients reflects the complexity of the interplay between the virus and the host, indicating that the course and outcome of COVID-19 are mainly determined by the reaction of the patient's immune system and the host-pathogen interactions.^[2] In some patients, COVID-19 disease can lead to uncontrolled production of pro-inflammatory cytokines, in a process known as cytokine release syndrome or cytokine storm (CK).^[3,4] The cytokine storm associated with the pathogenesis of the SARS-CoV-2 infection has been clinically characterized in depth,^[4,5]; however, translation of the infection to animal models posed several limitations,^[6,7] including the differential expression of the main viral receptor (ACE2;^[8]), and also in the species-specific release of mediators of inflammation, such as NO,^[9–14]

In this context, the macrophage has been identified as a key factor in the inflammatory response and is the main cell type involved in the release of CK. As in recent years, growing evidence has pointed out that macrophage polarization is accompanied by metabolic rewiring,^[15] immunometabolism arises as a highly relevant component to be studied in the COVID-19 disease. Briefly, macrophages that are polarized toward an “M1-like”, pro-inflammatory phenotype, increase their glycolytic, pentose phosphate (PPP), and fatty acid synthesis (FAS) pathways, exhibit TCA cycle breaks at citrate and succinate, and reduced mitochondrial oxidative phosphorylation (OXPHOS), whereas “M2-like”, anti-inflammatory macrophages rely more on their OXPHOS, increase FAS and glutamine metabolism, and reduce PPP.^[16,17] Importantly, the first TCA break results in citrate accumulation, which is then converted into itaconate, a metabolite that exhibits antimicrobial activity.^[18] In this regard, NO is considered a pro-inflammatory inducer, inhibiting OXPHOS while increasing glycolysis,^[19] and lipid accumulation and showing TCA break at citrate,^[20,21] These immunometabolic changes have been studied in SARS-CoV-2 infections, where the response of the macrophage is similar to other viral infections. Specifically, the TCA cycle flux is reduced, while glycolysis is highly increased, which is mediated by an increase in the production of ROS and HIF-1 α stabilization.^[22] Furthermore, a study showed

that purine, pyrimidine, nicotinamide, tryptophan, and arginine metabolisms were altered in COVID-19 patients' serum.^[23]

Regarding “M1-like” macrophage production of NO, current knowledge in the area of infectious diseases confirms that this molecule plays a relevant role in the regulation of the host defense and the inflammatory response.^[17,24–28] However, one of the main differences between human and classic rodent animal models' response to viral or bacterial infections is the reduced or even absent expression of NOS2 by the innate immune system of the high-throughput nitric oxide synthase (NOS2).^[26,29,30] The levels of NOS2 expression and activity are mainly regulated at the transcriptional level and this deficiency in its expression can be explained through several mechanisms including the different structure of the human NOS2 promoter, which expands up to 16 kb in humans versus *ca.* 2 kb in rodents.^[30]; and to epigenetic modifications, which restrict the rapid transcriptional control required to cope with the early phases of the infectious process.^[26,30–32] In addition, polymorphisms in a (CCTTT)*n* repeat in the human NOS2 promoter,^[33] and the presence of selective interfering miRNA, such as miRNA-939,^[34] have been identified as additional NOS2-suppression mechanisms. Interestingly, NO can be delivered by different means, and hyperventilation in the presence of NO has not been clinically explored in depth as a strategy to reduce SARS-CoV-2 replication and, simultaneously improve the patient's respiratory efficiency,^[9,35,36] In fact, in addition to the improvement of inflammatory signaling exerted by NO, it has been recognized that the protection of the host against pathogens is a primary effect of this radical and its derivatives, such as peroxynitrite.^[13,14,37,38] The potential role of exogenous administration of NO, either via ventilation/inhalation or by NO-donors has been proposed as a therapeutic agent at different levels,^[10,14,36,39]; however, the clinical trials devoted to this intervention have not provided definitive conclusions,^[40] including the prevention of infection upon nasal administration of NO (the Nitric Oxide Nasal Spray as Prevention for Treatment of Individuals at Risk of Exposure to COVID-19 Infection, NONS, NCT05109611, and the NOSARSCOVID, NCT04290871).

Thus, we have evaluated in primary cultures of human macrophages (hM ϕ) the impact of NO administration, via a sustained chemical NO donor, on the immunometabolic response of hM ϕ challenged with the cytokines characteristic of the “cytokine storm” observed in COVID-19 patients.^[3–5,41] Our data show that NO significantly alters the transcriptomic and fluxomic profiles of hM ϕ after exposure to the cytokine storm, and suggest that strategies based on NO administration to COVID-19 patients deserve further attention and specific clinical trials.

2. Results

2.1. NO Protects Human Macrophages (hM ϕ) Against Apoptosis-Induced COVID-19 Cytokine Storm (CK)

To induce a pro-inflammatory stimulus that resembles the COVID-19-induced cytokine storm, we revised the different analyses and meta-analyses published at that moment.^[42–44] We identified IL1 β , IL6, IL8, GM-CSF, IFN γ , and TNF α as the most common cytokines throughout the literature, and therefore decided to use all of them as our cytokine stimuli (CK). Activation of hM ϕ with these cytokines and/or the long-lasting NO-donor

S. Madurga, N. Aleixandre
Department of Material Science and Physical Chemistry & Research
Institute of Theoretical and Computational Chemistry (IQTCUB)
University of Barcelona
Barcelona 08028, Spain

A. Castrillo, J. V. de la Rosa, L. Boscá
Unidad de Biomedicina (Unidad Asociada al CSIC) de la Universidad de
Las Palmas de Gran Canaria
Las Palmas 35016, Spain

A. Castrillo, J. V. de la Rosa
Instituto Universitario de Investigaciones Biomédicas y Sanitarias
(IUIBS) de la Universidad de Las Palmas de Gran Canaria
Las Palmas 35016, Spain

P. Prieto
Departamento de Farmacología, Farmacognosia y Botánica
Facultad de Farmacia, Universidad Complutense de Madrid
Madrid 28040, Spain

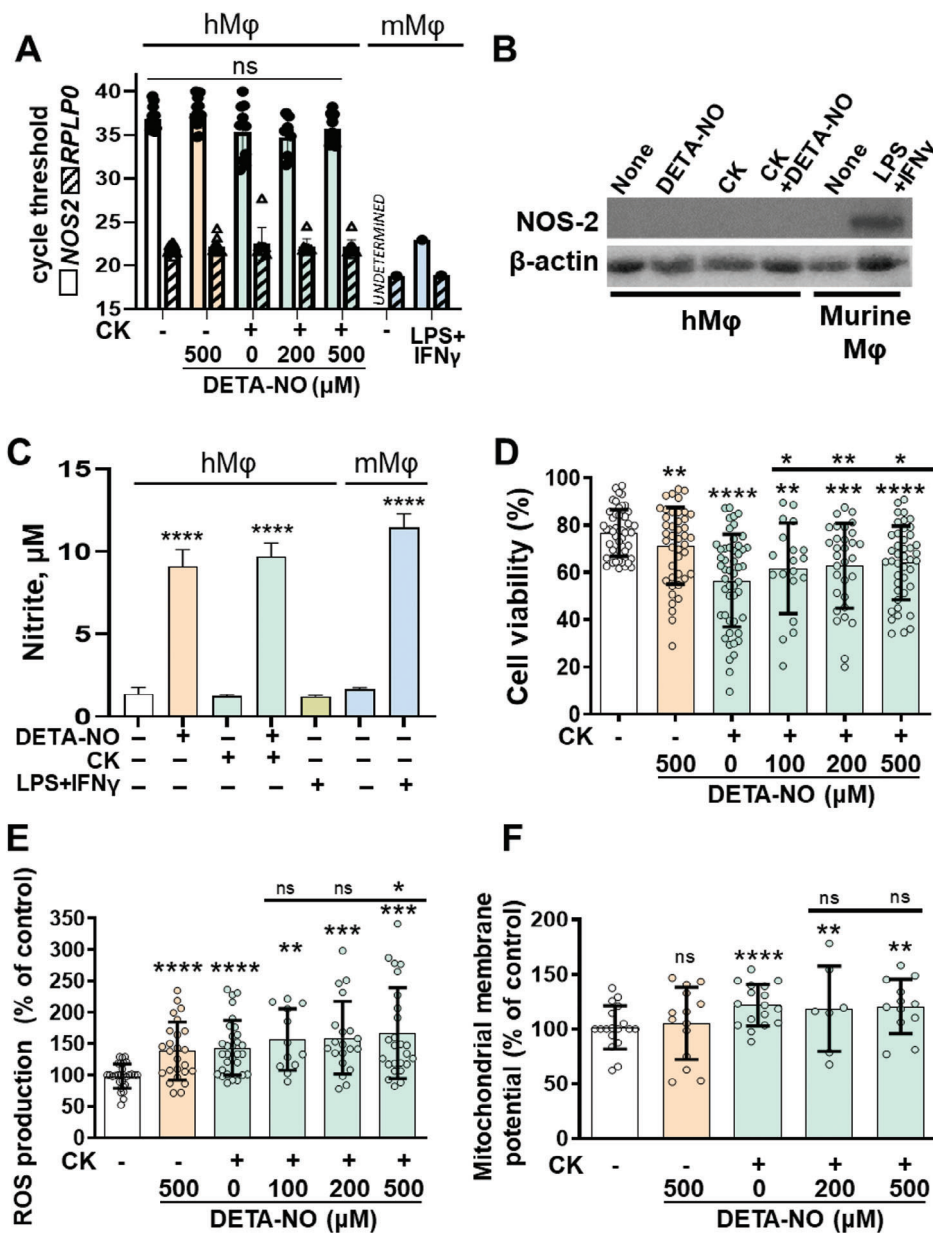


Figure 1. Cytokine (CK) administration to hMφ fails to induce a significant NOS2 expression but increases ROS production and mitochondrial inner membrane potential. Effect of incubation with the NO-donor DETA-NO. Human and murine Mφ (2×10^6 cells) were treated as indicated in the corresponding panels. A) Results show the RT-qPCR cycle thresholds of NOS2 and the normalization gene RPLP0 in human and murine Mφ after 24 h of incubation with the indicated stimuli; B) representative Western blot analysis of NOS-2 in human and murine Mφ after incubation for 24 h with 500 μM DETA-NO and/or CK. LPS and IFN- γ were used at $1 \mu\text{g mL}^{-1}$ and 20 ng mL^{-1} , respectively, as a positive control; the levels of β -actin were used as a normalization for lane charge. C) Nitrite accumulation in the culture medium of human and murine Mφ corresponding to panel B. D) Cell viability; E) ROS production; F) mitochondrial membrane potential (determined by CMXRos fluorescence intensity, in %) of hMφ after 24 h of treatment with the indicated stimuli. Results show the mean \pm SD of at least 10 distinct donors, or a representative blot (B). CK represents 20 ng mL^{-1} each of IL-1 β , IL-6, IL-8, TNF α , GM-CSF, and IFN γ . * $p < 0.05$; ** $p < 0.01$; *** $p < 0.001$; **** $p < 0.0001$ versus untreated cells or the 500 μM DETA-NO condition (CK samples); ns, not statistically significant.

DETA-NO did not induce the expression of human NOS2 at the mRNA (Ct values ≥ 36 –38; **Figure 1A**), protein, and activity levels (determined by the accumulation of nitrite in the culture medium; **Figure 1B,C**). The same results were obtained when using the well-known NOS2-inducing stimuli LPS and human IFN γ . In contrast, murine Mφ under these conditions experience

a robust induction of NOS2. The Ct value for NOS2 in RT-qPCR goes from undetectable (UNDETERMINED) to 23 (**Figure 1A**), a clear band can be observed in Western Blot versus no band in the control condition (**Figure 1B**) and there is a 7-fold increase in the production of nitrite (the end product of NO) (**Figure 1C**). In fact, the accumulation of nitrite in the culture medium was in the

same range as that liberated by DETA-NO in hM ϕ (Figure 1C). Moreover, treatment of hM ϕ with CK for longer periods (48 and 72 h) did not induce any NOS2 protein expression either (Figure S1, Supporting Information). Therefore, DETA-NO, a sustained NO donor, was used to evaluate the role of this molecule on the response of hM ϕ exposed to the COVID-19 cytokine storm (CK). The kinetics of NO release by this compound was determined using a NO-sensitive electrode, which ensured that DETA-NO provided a continuous availability of NO of 0.52 ± 0.07 from 1 mM of DETA-NO in the culture medium (half-life *ca.* 20 h; not shown). As Figure 1D shows, treatment with either DETA-NO or CK induced cell death in hM ϕ , which was higher in the latter one. However, pre-treatment of hM ϕ with concentrations between 100 and 500 μ M DETA-NO conferred significant protection of cell viability in cells treated with CK. The cell viability was determined by annexin V staining, suggesting apoptotic cell death. Both DETA-NO and CK significantly increased ROS production; however, only at 500 μ M DETA-NO did the ROS production by CK-treated cells further increase (Figure 1E). Since NO can affect the mitochondrial inner membrane potential,^[45] this parameter was measured with CMXROS probe and it exhibited a moderate, but statistically significant increase in cells treated with CK (Figure 1F). Neither the mitochondrial ROS production (determined with MitoSOX) nor the mitochondrial mass content (determined with Mitogreen) changed regardless of the presence of CK and/or DETA-NO (Figure S2, Supporting Information).

2.2. NO Changes hM ϕ Central Metabolism After Treatment with CK

The effect of CK and NO on glucose and lactate release to the cell culture medium after 24 h was assessed. Treatment of hM ϕ with DETA-NO did not modify the basal glucose consumption or the increased glycolytic flux elicited by CK (Figure 2A). Lactate accumulation in the medium showed a parallel profile to glucose consumption (Figure 2A). The lactate/glucose ratio in the medium decreased at 12–24 h of incubation in cells treated with CK regardless of the presence of NO (Figure 2B). It is worth mentioning the observed biphasic glycolytic behavior; the CK-dependent glucose consumption and lactate accumulation changed the shape after 12 h of treatment (Figure 2B); similar to the behavior observed in murine M ϕ ,^[17] As expected from previous work,^[19,46] the oxygen consumption rate (OCR) in the presence of NO was significantly reduced due to the inhibition of the cytochrome oxidase by NO (Figure 2C). In addition, CK treatment also significantly reduced the OCR, an effect that was enhanced in the presence of the NO donor. No statistically significant changes were observed in the metabolism of glutamine (data not shown).

2.3. NO has a Dose-Dependent Effect on the mRNA Levels of Immunometabolic Genes in hM ϕ Treated with CK

The effect of NO on the transcriptional regulation by CK was investigated focusing on the expression of genes that are involved in the inflammatory activity of hM ϕ . This analysis included the quantification of the levels of *TLR4* and the genes that modulate hM ϕ inflammation (*TNF*, *IL10*, *IL10R*, and *IL12B*), as well

as the G-protein-coupled receptors *SUCNR1* (which senses succinate and participates in different steps of the inflammatory process^[47]) and *GPR132* (highly expressed in hM ϕ and involved in the alternative polarization and neutrophil efferocytosis,^[48]), and the genes controlling hM ϕ -mediated immune suppression *CD274*, the gene encoding PD-L1, a protein involved in the regulation of the myeloid/lymphoid immune network, and *PDCD1LG2* (also known as *CD273* and coding for PD-L2),^[49] Treatment of hM ϕ with DETA-NO only increased the mRNA levels of *SUCNR1* among the analyzed genes in Figure 3, and *HIF1A*, *PFKFB3* (encoding PFKFB3, a HIF-1 α -dependent gene involved in the enhanced glycolytic flux in activated hM ϕ ,^[19]) and *LDLR* (the receptor of LDL, which is highly expressed in hM ϕ) of those shown in Figure S3 (Supporting Information). CK treatment of hM ϕ enhanced the mRNA levels of the genes involved in inflammation and reported in Figure 3, except the levels of *IL10* which were repressed. Indeed, the presence of NO did not alter the CK-dependent transcription profile, except for *IL10*, which was enhanced (Figure 3). Finally, the remaining genes analyzed in Figure S3 (Supporting Information) showed no relevant changes, except *SCARB1* which was significantly repressed in the presence of CK.

2.4. NO Treatment of hM ϕ Influences the CK-Dependent Transcriptomic Profile

The effect of treatment with DETA-NO, CK, and the combination of both on the transcriptomic profile of hM ϕ was analyzed. As Figure 4 shows, treatment with CK upregulated 813 genes and downregulated 618 of the differentially expressed genes (DEG). Of these genes, 25 and 6 genes respectively, were common when hM ϕ were treated with DETA-NO. More interestingly, 129 genes were upregulated in the presence of CK+DETA-NO versus the CK condition. In addition, 125 genes upregulated by CK were not present in the CK+DETA-NO condition. Regarding the repressed genes, 112 genes were specifically downregulated by CK+DETA-NO, whereas 239 were selectively downregulated by CK in the absence of DETA-NO. These results indicate a moderate effect of NO on the transcriptional control exerted by CK; however, NO, in addition to modulate the transcriptomic profile of hM ϕ , can modulate protein function via nitrosylation and nitration reactions,^[45,50]

Analysis of the clustering of these genes showed specific profiles associated with each treatment that can be grouped into 3 different clusters (Figure S4A, Supporting Information). Detailed comparisons of the top 50 genes modified in response to the different treatments are shown in Figure S5A–D (Supporting Information). It is remarkable that among the top genes enhanced in the CK plus DETA-NO condition (Figure S5C, Supporting Information), are the receptor adapter *JAK2* and the *SLAMF7* plasma cell marker (also known as CD319), of the Slam protein family, which is involved in T cell activation,^[51] Also, the exonuclease *XRNI*, which plays a role in RNA activation of the translation of plasma membrane proteins,^[52] and genes related to the IFN γ response (*ZNF1* and *GBP2*) and chromatin remodeling through the organization of the nucleosomes *BAZ1A*,^[53] were upregulated. Furthermore, the comparison of CK plus DETA-NO versus CK (Figure S5D, Supporting Information) shows the

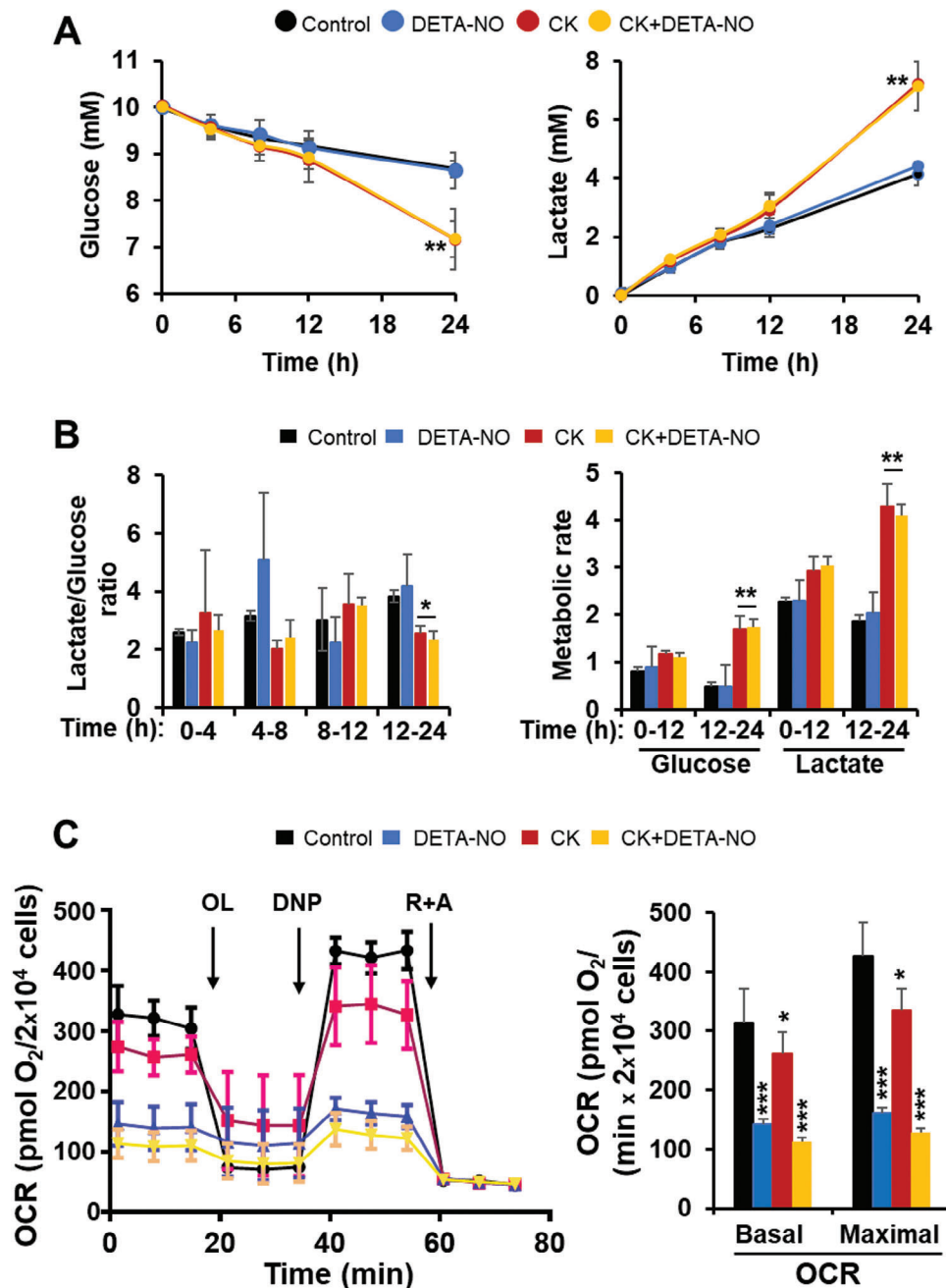


Figure 2. Effect of DETA-NO administration on glucose and oxygen consumption in $hM\phi$ upon cytokine storm (CK) treatment. A) Cells (2×10^6) were cultured in RPMI1640 medium and 2% FCS, and incubated with $500 \mu\text{M}$ DETA-NO and CK. The glucose consumption and lactate accumulation were determined in the culture medium at the indicated times. B) The ratio between glucose consumption and lactate accumulation was determined for the indicated periods as a measure of the glycolytic flux from glucose to lactate (left panel), while the metabolic rate was calculated by subtracting the concentrations of each metabolite at the indicated times. Metabolic rate is shown as absolute values (right panel) C) The oxygen consumption rate (OCR) after 24 h of treatment of $hM\phi$ (2×10^4 cells well^{-1}) with the indicated stimuli was assayed in a Seahorse XF platform. At the indicated times oligomycin (OL), 2',4'-dinitrophenol (DNP), and rotenone plus antimycin (R+A) were added. The basal and maximal respiration rates were quantified (right panels). Results show the means \pm SD from 7 different healthy donors assayed by triplicate. * $p < 0.05$; ** $p < 0.01$; *** $p < 0.001$ versus the corresponding untreated condition.

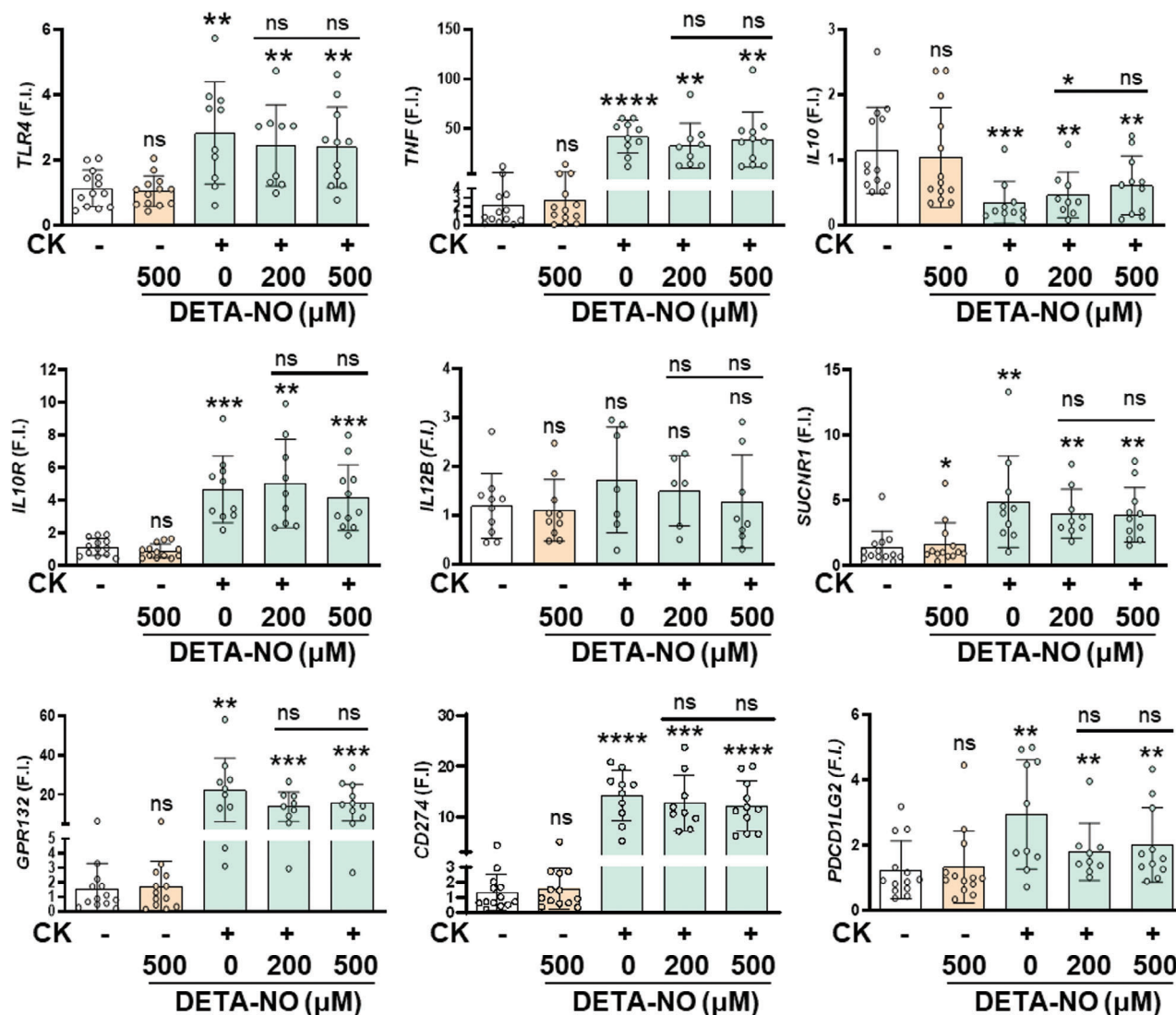


Figure 3. Regulatory effects of DETA-NO and CK on the expression of inflammation-related genes in hM ϕ . hM ϕ (10^7 cells per condition) from healthy donors were incubated for 24 h with the indicated stimuli and the RNA was isolated and analyzed by RT-qPCR. Results show the mean \pm SD of fold induction (F.I.) from 10 different donors assayed per triplicate. * $p < 0.05$; ** $p < 0.01$; *** $p < 0.001$; **** $p < 0.0001$ versus the untreated condition, or the DETA-NO condition (upper values). ns, not statistically significant.

upregulation of *NPPC*, which is expressed in the bone marrow and lymphoid tissues; *WNT6*, which is involved in the development and tissue homeostasis; and *DLL4* of the Notch pathway that participates in the proinflammatory activation of hM ϕ . Among the most repressed genes in the CK plus DETA-NO versus the CK condition, are the *H4C15* gene, which encodes for a replication-dependent histone of the H4 family; *KCND3*, which encodes for a potassium voltage-gated channel expressed in cardiac M ϕ and involved in the onset of atrial fibrillation; and *CCDC81* (coiled-coil domain containing 81) expressed in M ϕ and whose function in these cells remains poorly defined.

Furthermore, among the top canonical pathways that are modified in the DETA-NO+CK versus the CK samples (Figure 5), some changes are worth mentioning. In the upregulated pathways, the regulation of the Nrf2 pathway is the one that varies the most, and different Nrf2-related processes are modified.

In addition to this, the p53 pathway also appears upregulated, highlighting the potential for cross-regulation of the Nrf2-p53 pathways.^[54] On the other hand, responses to IFN γ and IFN α are repressed, along with oxidative phosphorylation and IL6/JAK/STAT3 signaling. Interestingly, pathways related to the maturation of SARS-CoV-2 spike protein and translation of SARS-CoV-2 structural proteins were also downregulated.

The 2D plots showing the individual overlapping between the different experimental conditions of treatment show the impact of NO on CK transcription when compared with the control condition (Figure S4B, Supporting Information). The overlapping between the DETA-NO+CK versus the CK condition is probably reflecting changes in the quantitative transcription of genes over the cut-off thresholds (Figure S4B, Supporting Information).

Figure S6A,B (Supporting Information) shows the Volcano and Venn diagrams associated with the different transcriptomic

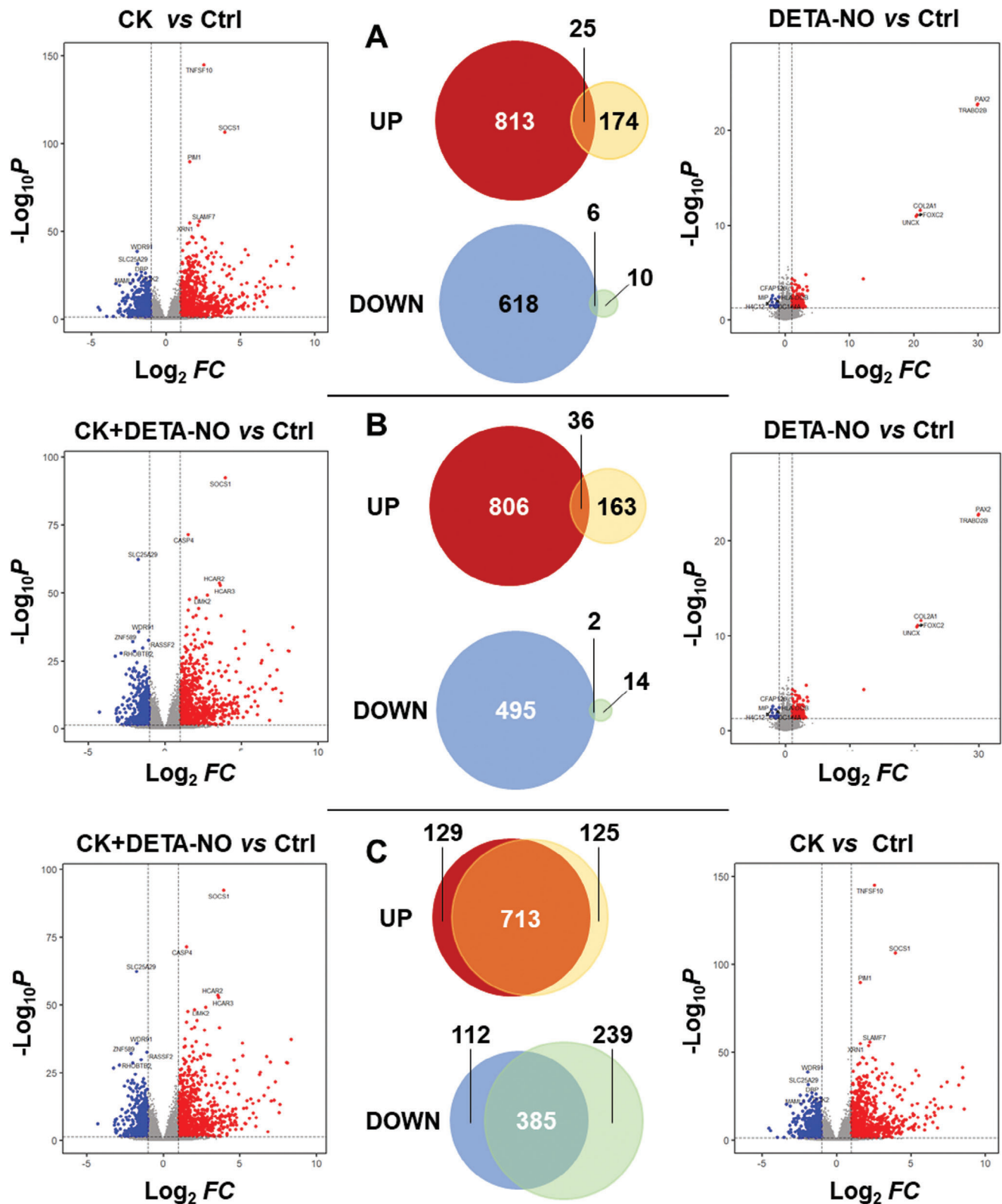


Figure 4. RNAseq gene expression analysis of hMφ after treatment with DETA-NO and CK. Results show the Volcano plots of all quantified genes in the transcriptome analysis of 10^7 hMφ per condition (24 h of treatment), and the corresponding Venn diagrams (up- and down-regulated genes) to define the specificities of each treatment (untreated control, 500 μ M DETA-NO and CK). Statistically significant differentially expressed genes (up- or down-regulated; red and blue colors, respectively) are defined as those with at least $\pm 30\%$ change (vertical lines in the Volcano plots) and $p < 0.05$. Volcano plots were generated as the mean \log_2 of fold change versus $-\log_{10}$ of hMφ p-values from 10 distinct healthy donors.

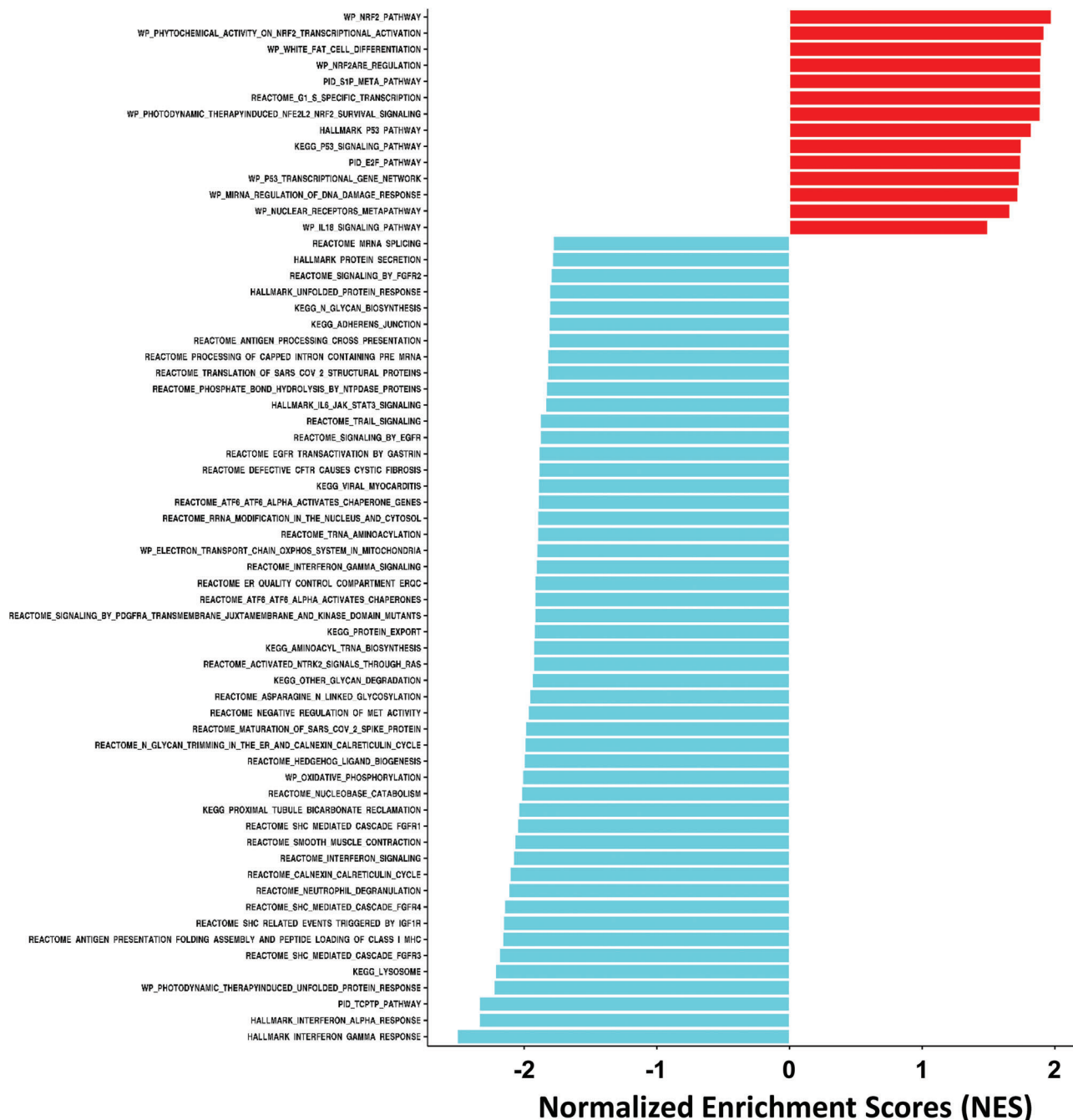


Figure 5. Top canonical pathways modified in hMφ treated with DETA-NO plus CK versus CK. Upregulated and downregulated canonical pathways with a higher normalized enrichment score (NES), in absolute value.

profiles and the main biological processes that are predicted to be altered as a result of the transcriptomic changes. Among the upregulated biological processes treatment with DETA-NO+CK exhibited an enhancement in pathways not covered by CK treatment. Specifically, the NF-κB pathway which is significantly activated upon CK treatment, is restricted in the presence of DETA-NO, which confirms previous proteomic and functional studies,^[55]

2.5. DETA-NO Treatment of hMφ Modifies the Fluxomic Profile Induced by CK

Flux analysis was conducted by integrating transcriptomics, metabolomics, and respiration data into the generic human Genome-Scale Metabolic Model (GSMM) Recon3D,^[56] as a template for the reconstruction of GSMMs of hMφ under control conditions, and DETA-NO, CK, and CK+DETA-NO treatments.

GIM3E and previously implemented algorithms,^[20,57,58] were applied to simulate the control and treatment-specific flux maps for the KEGG-defined metabolic pathways (<https://www.kegg.jp/>). The detailed metabolic analysis revealed that the pathways that present significant flux changes, upon the different treatments, are related to carbohydrate, TCA, OXPHOS, nucleotide, fatty acids, and amino acids metabolism (Figure 6). Furthermore, the obtained results via GSMM were in the same range as those obtained using the qMTA analysis (Figure S7, Supporting Information). Results show a dramatic increase in glycolysis and purine metabolism fluxes in response to either CK treatment or the combined treatment CK+DETA-NO, whereas DETA-NO only generates a slight increase (Figure 6A). The results of CK+DETA-NO treatment also show that DETA-NO treatment counteracts the increase of fatty acid metabolism and degradation induced by CKs. The pyrimidine and pyruvate metabolic pathways present a similar pattern of increased flux in all treatments, being slightly higher with DETA-NO treatment. The metabolism of glycine, serine, and threonine, and the metabolism of amino sugars and nucleotide sugars increase with CK treatment. These changes are reversed by CK plus DETA-NO, and even the NO treatment alone induces a slight decrease in these fluxes. The combined treatment also shows a synergistic effect by decreasing alanine, aspartate, glutamate, and pyruvate, whereas all the treatments induce a similar decrease in one-carbon metabolism flux. Analysis of additional specific metabolic pathways defined by GSMM Recon3D modeling is shown in Figure 6B. Here, it is worth mentioning the DETA-NO dependent repression in the OXPHOS pathway as experimentally observed from the data shown in Figure 2C, in the xenobiotic metabolism pathway, as well as in arginine biosynthesis and biotin metabolism. Detailed analysis of the individual steps in glycolysis, pentose phosphate pathway, and TCA are given in Figure 7. Remarkably, CK treatment results in an enhanced flux through the TCA cycle and OXPHOS metabolism and in a dramatic increase in itaconate production generated through reductive carboxylation (IDH2 reaction). These individual changes are represented in Figure 8. Moreover, these results show that NO neutralizes the impact of CK on TCA and OXPHOS also impairing itaconate production. These results are relevant in terms of hM ϕ metabolism, given the role that itaconate plays in these cells.^[18,59,60]

3. Discussion

The cytokine storm derived from the COVID-19 disease has entailed one of the greatest challenges since the outbreak of the SARS-CoV-2 virus began, being responsible for a large number of deaths and leading to a great socioeconomic burden. Still, nowadays, there is a lack of specific and effective treatments, which is why more research is required, especially since long-COVID cases are of high prevalence. In this regard, a relevant difference in the immune action of M ϕ between humans and most mammals used as animal models is the ability to synthesize NO through the expression of the high-throughput NOS2 enzyme. While murine and other species' macrophages synthesize large amounts of NO,^[61–63] hM ϕ produce little or no NO.^[64–66] Here, we strengthened this conclusion, as we did not observe NO production in PBMC-derived hM ϕ after either our “CRS-like” challenge or the classical pro-inflammatory stimuli LPS plus IFN γ .

Accordingly, we observed that hM ϕ failed to express NOS2 in response to proinflammatory activation, the main source of NO synthesis in other species.^[63] As NO has been recognized as an important molecule in “M1-like” polarization, the lack of production in humans could lead to “incomplete” polarization. Therefore, we sought to explore the effects of exogenous NO addition on hM ϕ immunometabolism in the CK context.

The “cytokine storm-like” model was established successfully, as shown by the changes in RNA expression. Thus, upon CK stimulation, the well-known pro-inflammatory genes *TNF*, *IL12B*, *SUCNR1*, *HIF1A*, and *PFKFB3* were all upregulated. The KEGG gene ontology functional annotation in the CK versus Control condition also supported our model. The classical IKK-mediated NF- κ B activation and the response to TNF α were upregulated, and several pro-inflammatory genes appeared among the top-50 genes, such as the interferon-induced genes *IRF1*, *GBP2* and *GBP5*; or *CASP4* that encodes for caspase 4, a protein involved in IL1 β processing and cell death.^[67] Moreover, the JAK2/STAT3 pathway components, which play an essential role in the inflammatory process by mediating the IL-6-derived response and activating the NLRP3 inflammasome, were upregulated.^[68] These mediators have been shown to highly contribute to the cytokine storm in COVID-19.^[69] Accordingly, the JAK/STAT negative feedback regulator *SOCS1* was increased.

Regarding M ϕ viability, NO can either promote or inhibit cell death depending on its concentration and time of exposure.^[38,70] Transient NO incubation can promote the release of cytochrome c from the mitochondria, which activates the intrinsic apoptotic pathway, while prolonged NO exposure inhibits caspase processing and activity and promotes the accumulation of inhibitors of apoptosis.^[70] Accordingly, our results show that DETA-NO, which provides a sustained release of NO, protects from CK-induced cell death. Indeed, the pathways related to the regulation of cell death and apoptosis were repressed as shown in the KEGG gene ontology functional annotation. Additionally, we observed that CK incubation increased ROS production. When M ϕ are polarized toward a pro-inflammatory phenotype, they increase the generation of ROS to fight against the infectious agent.^[63] Moreover, DETA-NO treatment further increased this ROS production. Surprisingly, neither CK nor NO changed mitochondrial superoxide production, which is interesting in view that superoxide is mainly formed from proton leakage in the mitochondria, and NO modifies the activity of many proteins of the OXPHOS pathway.^[71] These results suggest that NO would increase the ROS-mediated antimicrobial function of hM ϕ , while protecting them from cell death, thus improving the innate immune response. Moreover, the simultaneous presence of NO and superoxide rapidly generates peroxynitrite, one of the most powerful oxidants in living cells,^[72] which is used by macrophages to kill pathogens.^[72]

At the transcription level, RNAseq studies show that DETA-NO induced minimal changes in the RNA levels of genes involved in the regulation of inflammation or in the main metabolic pathways. There was a slight increase in both *PFKFB3* and *HIF1A*, which are positively regulated by each other and act to promote pro-inflammatory activation, mainly by increasing the production of cytokines such as IL-1 β .^[19] Previous studies showed that NOS inhibition resulted in decreased *PFKFB3* expression, and

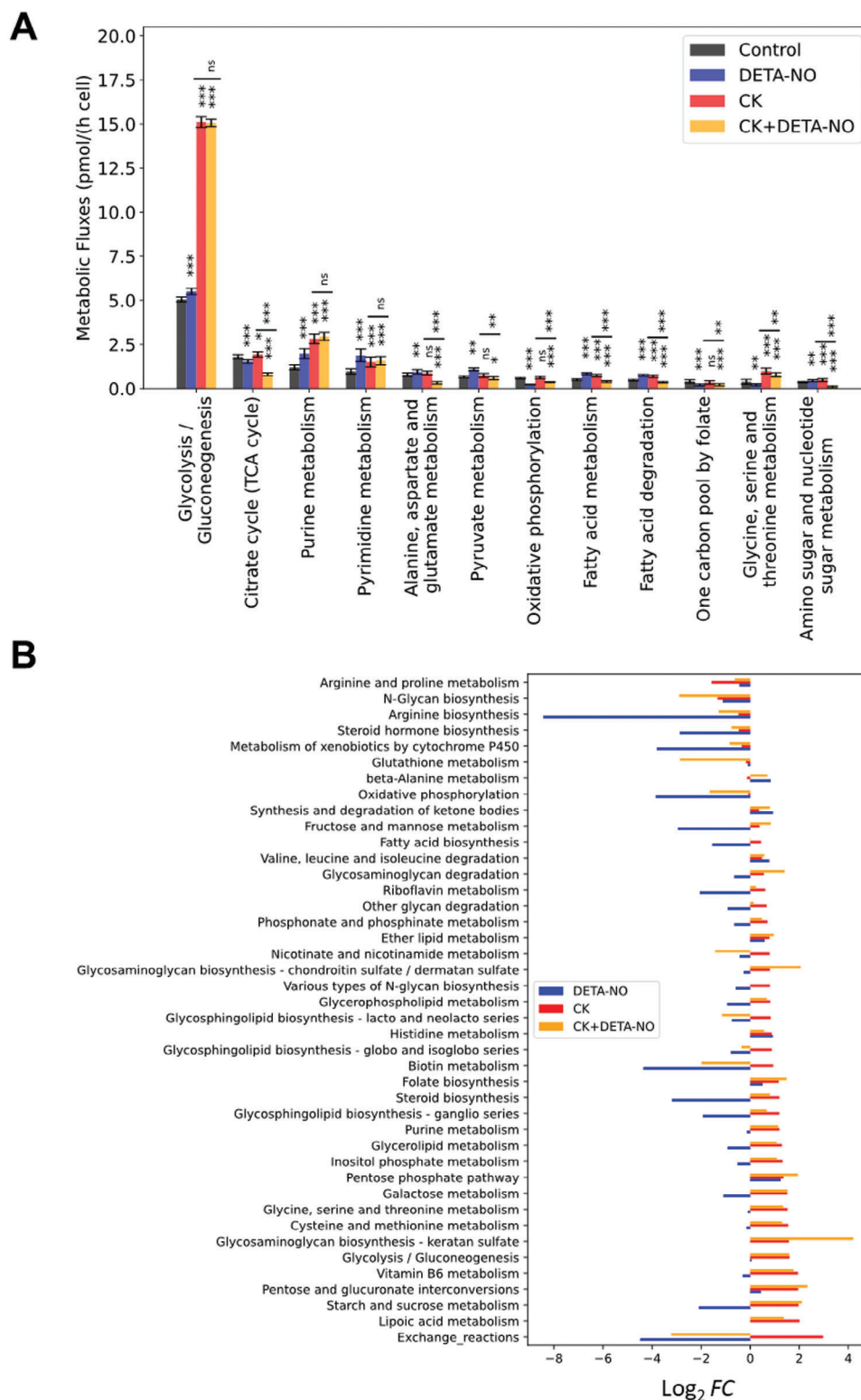
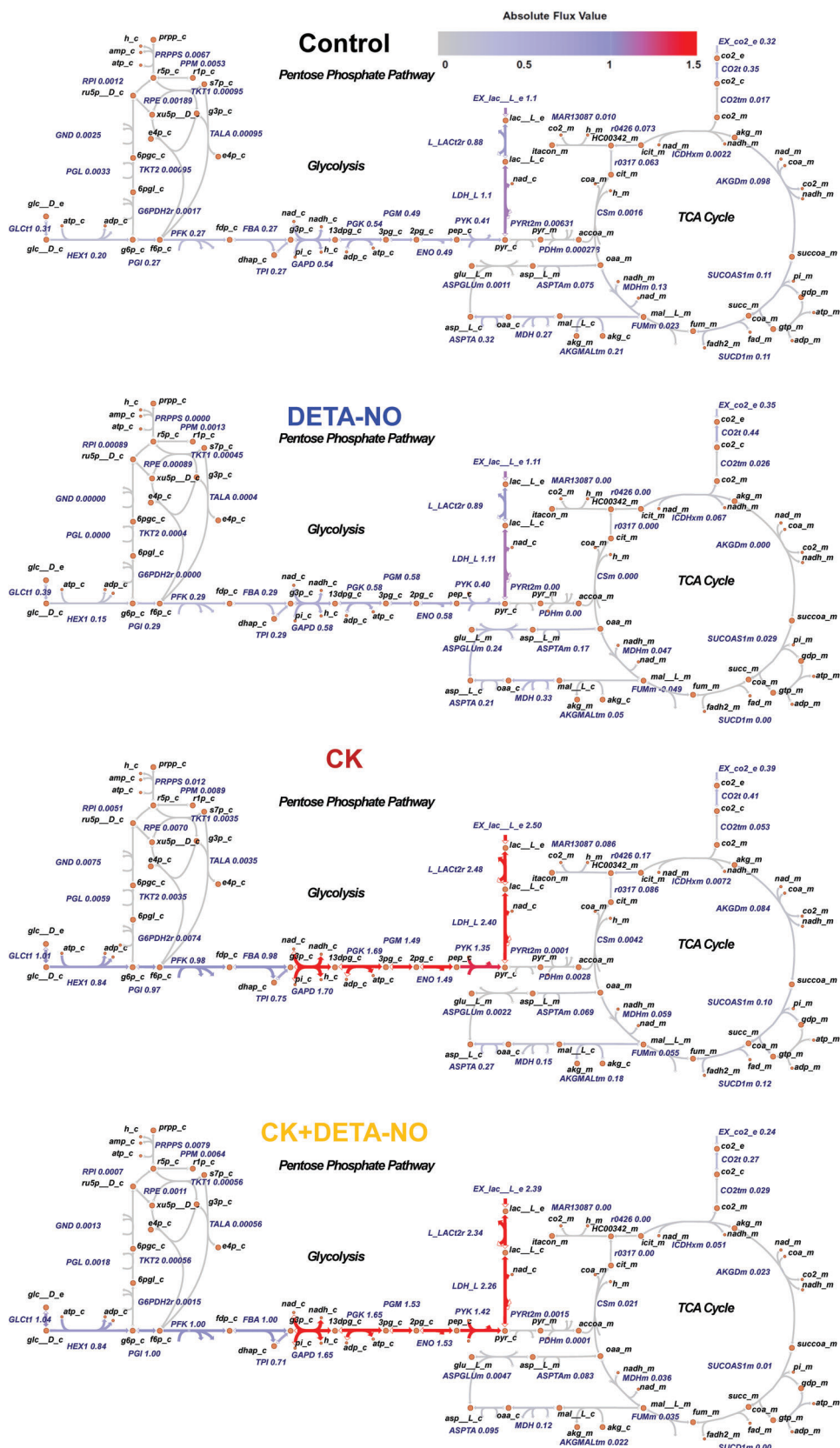


Figure 6. Modulation of metabolic fluxes predicted by human Genome-Scale Metabolic Model (GSMM) in *hMφ* treated with DETA-NO and CK. A) Distribution of metabolic fluxes across several pathways, as determined by the GIM3E algorithm and sampling procedure. B) Relative log₂ fold change of pathways among conditions determined from qMTA procedure. **p* < 0.05; ***p* < 0.01; ****p* < 0.001 (panel A) versus the control value or the CK condition (bar values). ns, not statistically significant.



the relationship between NO and HIF-1 α has been extensively described.^[24,73] Interestingly, treatment with DETA-NO produced a partial recovery of the CK-induced downregulation of *IL10*. This repression in *IL10* is controversial since different circulating levels of IL-10 have been described in COVID-19 patients.^[74] Moreover, specific changes were observed in the RNAseq study when comparing the CK plus DETA-NO versus the CK condition, which is reported in Figure S5D (Supporting Information). Briefly, this figure shows the upregulation of genes involved in macrophage migration and proliferation such as *GPR55*, *CTNND2*, and *WNT6* (i.e.,^[75]). Furthermore, *DLL4* was upregulated, which has been described to inhibit M2 macrophage differentiation and promote their apoptosis,^[76] while inducing pro-inflammatory polarization. However, this process is impaired by NO-dependent caspase inhibition.^[37,70]

Although these results support that DETA-NO induces a pro-inflammatory phenotype, a greater number of genes were related to an anti-inflammatory status. Special interest deserves *WNT6*, which upregulates Arg-1 and downregulates TNF α , promoting M2-like macrophage polarization,^[75]; and *PBX1*, which mediates IL-10 expression in macrophages upon apoptotic cell phagocytosis (efferocytosis).^[77] Indeed, the evaluation of the capacity of M ϕ to phagocytize zymosan exhibited a moderate, but statistically significant increase when comparing CK+DETA-NO versus CK (not shown). Among the most repressed genes was *PALM3*, which increases inflammation in alveolar macrophages treated with LPS,^[78]; and *OSMR*, which is expressed by M1 macrophages, and whose deficiency results in M2 macrophage polarization.^[79] In addition, analysis of top canonical pathways showed a DETANO-induced inhibition of IFN γ and IFN α responses, along with a decrease in the IL6/JAK/STAT3 signaling pathway. On the other hand, the top-upregulated pathways show an activation of Nrf2-related pathways, which are great antioxidant mechanisms. DETANO has already been shown to increase Nrf2 expression in murine macrophages,^[80] probably as a response to oxidative stress. However, NO can also directly affect the Nrf2 pathway through a post-translational S-nitrosylation of the Nrf2 inhibitor Keap1.^[80] Taken together, these results show that macrophages lead to an “M2-like” phenotype upon NO exposure.

Macrophages are essentially glycolytic cells and here, we observed that the treatment with DETA-NO did not alter the basal glycolytic flux; however, incubation with CK promoted biphasic changes, with an increased glucose consumption and lactate release to the culture medium that changed after 12 h of treatment. Under these conditions, the presence of NO did not modify the flux enhanced by CK. This biphasic behavior has also been observed in peritoneal M ϕ under pro-inflammatory conditions.^[17] Interestingly, from a metabolic perspective, one of the main effects of the NO released after the expression of NOS2 is the inhibition of OXPHOS at different points. Complexes I, II, III, and, more importantly, cytochrome C (Complex IV), are inhibited in the presence of NO. In the latter case, this inhibition is mediated by NO competition with O₂ for the heme domains.^[50,71,81] Our data show that NO inhibits basal respiration, as does CK-activated hM ϕ , which is likely related to an increase in glycolytic flux. Under our conditions, Gln consumption was very low and it was difficult to follow its metabolism. For this reason, we disregarded further analysis of the Gln metabolism. However, we cannot exclude that metabolites from the Gln pathway may participate in the metabolic profiling of hM ϕ .

Moreover, it is worth mentioning that NO inhibits key enzymes involved in the regulation of the TCA, in addition to the effects on the OXPHOS pathway, as well as cytoplasmic enzymes that share aminoacidic thiol residues (i.e., cysteine) or prosthetic groups, such as heme or [4Fe-4S] clusters.^[82,83] Aconitase, which is present in the cytoplasm (ACO1 isoenzyme) and in the mitochondria (ACO2), is one of the targets of NO that, after the inhibition, promotes a metabolic rewiring toward amino acid biosynthesis.^[20,82,84] In the case of M ϕ , this flow through aconitase is important since it can be bypassed to the synthesis of itaconate, an important metabolite in proinflammatory M ϕ polarization.^[18,59,60] This synthesis is mediated through the expression of aconitase decarboxylase, an enzyme that is highly expressed in hM ϕ by CK and encoded by *ACOD1* (log₂ fold change = 6.85). Moreover, in the presence of DETA-NO, the levels of *ACOD1* even increased (log₂ fold change = 7.34).

The obtained results from metabolic flux simulations using treatment-specific GSMMs unveiled the existence of reductive carboxylation through the reverse reaction of mitochondrial

Figure 7. Fluxes of glycolysis, pentose phosphate, and TCA cycle pathways in hM ϕ treated with DETA-NO and CK. Upregulated and downregulated reactions are indicated for Glycolysis, Pentose phosphate, and TCA cycle pathways. Reaction colors correspond to the average flux values obtained from the sampling procedure (units: 1884 pmol/(h-cell)). The thickness and color of the arrows are based on the flux values. Fluxes with values higher than 1.5 are assigned the maximum scale color. In the diagrams, the arrow indicates the direction of the flux. **Glycolysis:** HEX1: hexokinase 1; PGI: glucose-6-phosphate isomerase; PFK: phosphofructokinase; FBA: fructose-1,6-bisphosphate aldolase; TPI: triosephosphate isomerase; GAPD: glyceraldehyde 3-phosphate dehydrogenase; PGK: phosphoglycerate kinase; PGM: phosphoglycerate mutase; ENO: enolase; PYRt2m: mitochondrial pyruvate carrier; PDH: pyruvate dehydrogenase; LDH_L: L-lactate dehydrogenase; glc: glucose; g6p: glucose-6-phosphate; f6p: fructose-6-phosphate; fdp: fructose 1,6-bisphosphate; dhap: dihydroxyacetone phosphate; g3p: glyceraldehyde-3-phosphate; 13dpg: 1,3-bisphosphoglycerate; 3pg: 3-phosphoglycerate; 2pg: 2-phosphoglycerate; pep: phosphoenolpyruvate; pyr: pyruvate; lac_L: L-lactate; accoa: acetyl-coenzyme A; atp: adenosine triphosphate; adp: adenosine diphosphate; h: proton; nadh: nicotinamide adenine dinucleotide; nadph: nicotinamide adenine dinucleotide phosphate; pi: inorganic phosphate; coa: coenzyme-A; _c: cytosolic; _m: mitochondrial. **Pentose phosphate pathway (PPP):** G6PDH2r: glucose-6-phosphate dehydrogenase; PGL: 6-phosphogluconolactonase; GND: 6-phosphogluconate dehydrogenase; RPE: ribulose-phosphate 3-epimerase; RPI: ribose-5-phosphate isomerase; PPM: phosphopentomutase; TKT1: transketolase; TALA: transaldolase; glc: glucose; g6p: glucose-6-phosphate; f6p: fructose-6-phosphate; 6pgl: 6-phosphogluconate; ru5p: ribulose-5-phosphate; r5p: ribose-5-phosphate; r1p: ribose-1-phosphate; xu5p: xilulose-5-phosphate; s7p: sedoheptulose-7-phosphate; e4p: erythrose-4-phosphate; g3p: glyceraldehyde-3-phosphate; h: proton; nadh: nicotinamide adenine dinucleotide; nadph: nicotinamide adenine dinucleotide; _c: cytosolic. **TCA:** CS: citrate synthase; r0317 and r0426: aconitase 1 or 2; MAR13087: aconitase decarboxylase; ICDH: isocitrate dehydrogenase; AKGD: α -ketoglutarate dehydrogenase; SUCOAS1: succinate synthase; DIC: dicarboxylate carrier; SUCD1: succinate dehydrogenase; FUM: fumarate; MDH: malate dehydrogenase; accoa: acetyl-coenzyme A; coa: coenzyme A; cit: citrate; HCO0342: cis-aconitate; itacon: itaconate; icit: isocitrate; akg: α -ketoglutarate; succoa: succinyl-coenzyme A; succ: succinate; so3: sulfite; gtp: guanosine triphosphate; gdp: guanosine diphosphate; pi: phosphate inorganic; fum: fumarate; mal: malate; oaa: oxaloacetate; h: proton; nadh: nicotinamide adenine dinucleotide; fadh2: flavin adenine dinucleotide; _c: cytosolic; _m: mitochondrial.

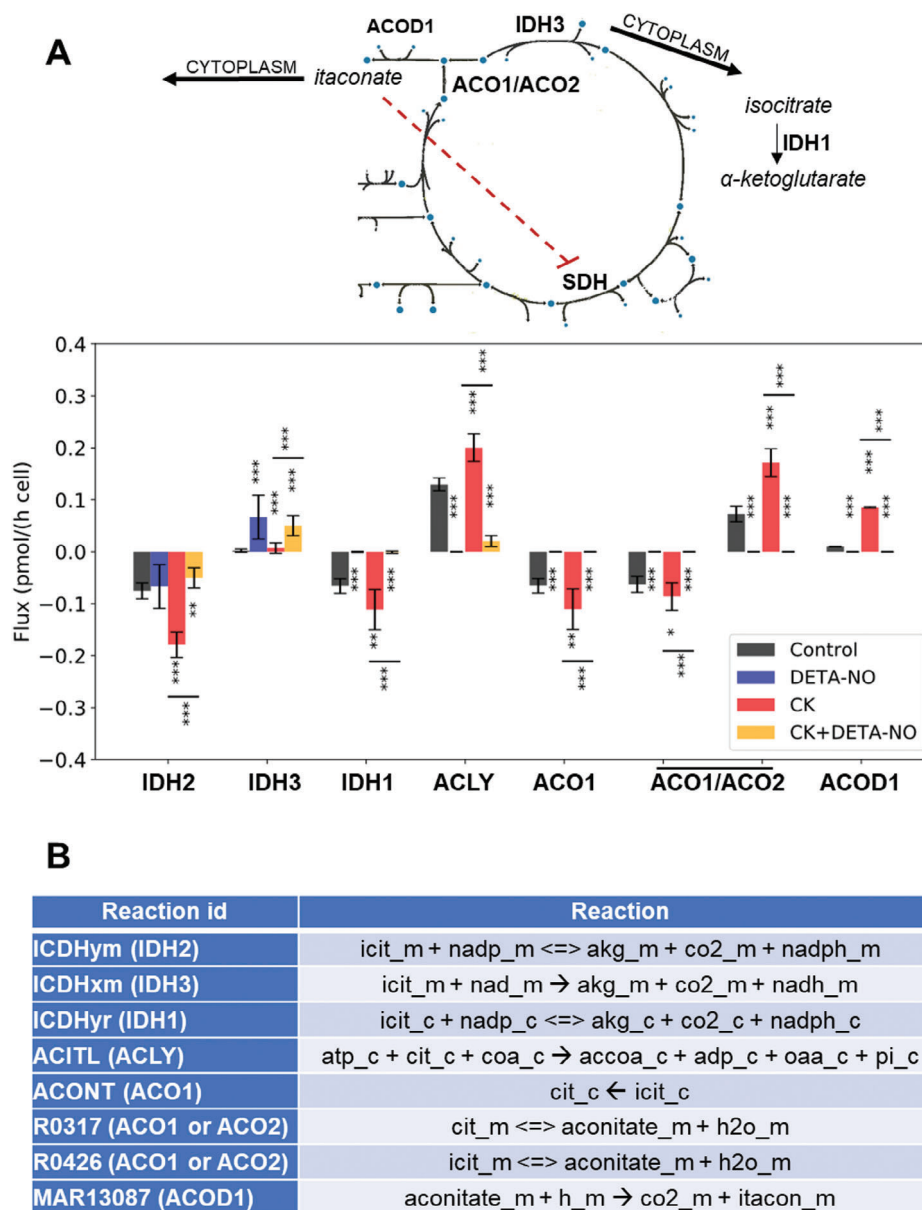


Figure 8. Analysis of the modulation of itaconate synthesis pathway by human Genome-Scale Metabolic Model (GSMM) in hMφ treated with DETA-NO and CK. (A) Schematic representation of itaconate synthesis. The effect of DETA-NO on the aconitase activity was calculated using the GSMM ReconD3 algorithm and expressed as average flux values obtained from the sampling procedure. (B) Description of the individual reactions used to establish the GSMM analysis. (A) Results show the mean ± SD of the corresponding values expressed as “relative flux”. * $p < 0.05$; ** $p < 0.01$; *** $p < 0.001$ versus the control value or the CK condition (bar values). ns, not statistically significant.

isocitrate dehydrogenase (IDH2), which is the main source of *cis*-aconitate to produce itaconate through aconitate decarboxylase (MAR13087, encoded by ACOD1). This enzyme is highly overexpressed after CK treatment. These results agree with those experimentally observed in hMφ by Heinz et al., 2022, using appropriate ^{13}C -labeled substrates.^[85] Analysis of the DETA-NO treatment in the GSMM study includes the inhibitory effect of NO on aconitase and cytochrome c oxidase, supporting the role of these specific inhibitory effects of NO on OXPHOS enhancement and the overproduction of itaconate triggered by CK. These results imply that the absence of NO in the case of hMφ pro-inflammatory ac-

tivation, due to the lack of NOS2 expression, favors the accumulation of itaconate, which would inhibit succinate dehydrogenase (SDH), increasing the levels of succinate and, therefore, decreasing HIF-1α. Moreover, itaconate, due to its α,β-unsaturated dicarboxylic nature, can modify cysteine residues via Michaelis' addition reactions while reducing oxidative stress (stabilizing Nrf2), inhibiting type I IFN expression,^[86] and improving immune tolerance and hMφ metabolism.

Altogether, the results described in this study suggest a dual immunomodulatory effect of NO in Mφ. On the one hand, NO increased ROS production, the glycolytic pathway, reduced

OXPHOS, upregulated the pro-inflammatory genes *HIF1A* and *PFKFB3*, and reduced itaconate biosynthesis. On the other hand, it inhibited CK-induced cell death, induced the transcription of anti-inflammatory genes, increased the Nrf2 pathway, and down-regulated the IFN γ and NF- κ B pathways. Furthermore, here we show that the enhancement of TCA and itaconate production pathways induced by cytokine storm is neutralized by NO. Although the M ϕ cell fate depends on a huge variety of factors, such as the environment and NO concentrations, we hypothesize that NO ameliorates the fight against pathogens such as SARS-CoV-2, while preparing M ϕ to transit to a resolution phase, where inflammation is blunted, and homeostasis is restored.

4. Conclusion

It has been extensively reported that NO levels (synthesized by constitutive NOS1 and NOS3) and bioavailability are decreased in patients with COVID-19.^[28,87] Therefore, supplementation of NO has been suggested as an alternative treatment for COVID-19 patients due to its vasodilator, anticoagulant, anti-inflammatory and antiviral properties.^[9,28,87] Several clinical trials are ongoing which increases the interest in further exploring the underlying molecular mechanisms of NO-based therapy against SARS-CoV-2. One example is the multicenter phase II trial based on the administration of inhaled NO to treat acute hypoxemic respiratory failure in COVID-19 patients.^[88] Together, these results reveal new putative mechanisms for the potential advantages of NO therapies that are expected to lead to advances not only in the treatment of COVID-19 but also in other diseases, such as prolonged sleep deprivation that induces a similar profile to the cytokine storm.^[89]

5. Experimental Section

Materials: Reagents were from Merck (Darmstadt, Germany) or Roche (Darmstadt, Germany). Cytokines were obtained from PeproTech (London, UK). Reagents for electrophoresis were from Bio-Rad (Hercules, EEUU). Tissue culture dishes were from Falcon (Lincoln Park, NJ, USA), and serum and culture media were from Invitrogen (Life Technologies/Thermo-Fisher, Madrid, Spain).

Isolation of Human Monocytes and Preparation of Human Macrophages: Human monocytes were obtained from peripheral blood from anonymous healthy donors, following the Centro de Transfusiones de la Comunidad de Madrid agreements (28 504/000011). Clear information was given to all the contributors, who provided written consent in agreement with the 1975 Declaration of Helsinki and the Committee for Human Subjects. The procedure followed was the same as previously described.^[90] In brief, the blood concentrate was slowly added dropwise over a Ficoll (17–0300, Sigma–Aldrich-GE) layer and centrifuged for 25 min at 450g at RT in a centrifuge with no break. Then, the buffy coat layer was collected in a new tube, washed twice with PBS, and centrifuged for 5 min at 300g. Residual erythrocytes were lysed by incubating with red blood lysis buffer (420 302, Biolegend) for 10 min and then washing twice with PBS. Cell count and viability were addressed in a flow cytometer (Cytotrex-S, Becton Dickinson) using 2 μ M DAPI fluorescent probe (D1306, Invitrogen). After that, PBMC were centrifuged for 5 min at 300g and resuspended in serum-free DMEM (41966-029, Gibco) medium with 100 U mL⁻¹ penicillin and streptomycin (15140–122, Gibco), and then seeded at 1–2 \times 10⁶ cells well⁻¹ in 6-well culture plates or 10 \times 10⁶ cells in 100 mm plates (353 046, Falcon). Cells were maintained in serum-free medium for 1 h to induce monocyte cell adhesion. Then, plates were washed twice with PBS to remove cells in

suspension and isolate the monocytes only, and new DMEM was added, this time supplemented with 10% heat-inactivated FBS. Monocytes were maintained in these conditions until hM ϕ differentiation was evident by microscopy observation, which usually took 7 days to happen.

Isolation of Murine Peritoneal Macrophages: Murine M ϕ were obtained as previously described.^[91] Briefly, C57BL/6J wild-type (WT) mice were from Jackson Laboratory and bred in our research center's animal facilities. Animal experiments were conducted following Institutional and administrative requirements (PROEX 228_17). Experiments were conducted with regulated temperature and humidity and mice were exposed to 12 h light-12 h dark cycles. 8–12-week-old mice were injected intraperitoneally with 2.5 mL of 3% (w/v) thioglycolate broth,^[17] to recruit M ϕ to the peritoneal cavity. After 2 days, mice were sacrificed in a CO₂ atmosphere, and peritoneal M ϕ were obtained after injecting 10 mL cold RPMI 1640 (21 875, Gibco) into the peritoneum. Macrophages were then pelleted by centrifugation at 420g for 10 min at 4 °C. Then, M ϕ were resuspended in RPMI and 10% FBS and seeded in 6-well plates at a density of 3 \times 10⁶ cells well⁻¹ and let in an incubator at 37 °C and 5% CO₂. After incubation for 4–6 h, the medium was removed, non-adherent cells were discarded by washing thoroughly with PBS, and new RPMI with 10% FBS was added.

Cell Treatments: Before all experiments, hM ϕ were washed with PBS, and new RPMI supplemented with 2% FBS was added. Macrophages were then treated with the human recombinant proteins IL-1 β (200-01B), IL-6 (200-06), IL-8 (200-08), TNF α (300-01A), GM-CSF (300-03), and IFN γ (300-02; all from PeproTech and used at 20 ng mL⁻¹) for 1 h at 37 °C and 5% CO₂. After that, the NO donor DETA NONOate (DETA-NO; ALX-430-014, Enzo) was added, and the cells were incubated for another 24h. DETA-NO was used immediately after preparation. For the mice peritoneal M ϕ experiments, cells were also washed with PBS, and new RPMI with 10% FBS media was added. Cells were treated with 1 μ g mL⁻¹ LPS (L7261, Sigma) and 20 ng mL⁻¹ IFN γ for 24 h at 37 °C and 5% CO₂.

Flow Cytometry Assays: After treatments, cells were detached with Tryple Express (12604-013, Gibco) for 4 min at 37 °C and 5% CO₂, which was then neutralized using PBS with 2% FBS. Cells were gently scrapped off the dishes and centrifuged for 5 min at 300g at RT. Macrophages were incubated for 30 min at 37 °C with the following fluorescent probes: to measure ROS production, 5 μ M DCFH-DA fluorescent probe (2'-7'-dichlorofluorescein diacetate; D6883, Sigma) was used,^[92–94] for mitochondrial superoxide generation, 5 μ M MitoSOX (M36008, Invitrogen),^[95] to measure mitochondrial inner membrane potential ($\Delta\Psi$ m), 100 nM MitoTracker Red CMXRos (M7512, Invitrogen),^[45] Finally, to assay the mitochondrial mass, 100 nM MitoTracker Green FM (M7514, Invitrogen) was used. Cell viability was always assessed by incubation with DAPI for 5 min at RT,^[27,70,96] All experiments were carried out in a Cytotrex S (Becton Dickinson). Data were analyzed using CytExpert software.

Glucose and Lactate Determination: After treatment, hM ϕ supernatants were collected at different times and centrifuged at 2 000g for 10 min. Cell pellets were discarded and supernatants were kept at -80 °C until use. Metabolite concentrations were determined using NADP(P)H-coupled enzymatic reactions in an autoanalyzer Cobas Mira Plus (Horiba ABX).

Seahorse Measurements (Agilent Technologies XF24): Cells were seeded at a rate of 2 \times 10⁴ cells well⁻¹ in a 96-well Seahorse plate (103794-100, Agilent). After 24 h, cells received the corresponding treatments for the times previously stated. Measurement of Oxygen Consumption Rate (OCR) was realized in real-time in an eFlux Analyzer XF96 (Agilent), following the manufacturer's instructions. Briefly, cell media was removed, and cells were washed once with Seahorse media (DMEM with 10% FBS, 1% pyruvate, 1% glucose, 1% glutamine). Then, Seahorse media was added, and cells were incubated for 45 min (37 °C and 5% CO₂). A previously hydrated cartridge was introduced into the Seahorse analyzer for calibration. Then, the Seahorse plate was introduced, and respiratory chain inhibitors were sequentially added in the following order and at the indicated concentrations: 1 μ M oligomycin, 1 μ M FCCP (cyanide-p-trifluoromethoxyphenylhydrazone), and 0.5 μ M rotenone and antimycin A (Merck). A minimum of 4 wells were used for each experimental replicate. Results were analyzed using the Agilent Seahorse Wave Software.

Protein Extraction and Western Blot: Cells were homogenized in extraction buffer (10 mM Tris-HCl; pH 7.5, 1 mM MgCl₂, 1 mM EDTA, 0.5% CHAPS, 10% glycerol) containing protease and phosphatase inhibitors (P8340, P5726, P0044, Sigma). Homogenates were then vortexed for 30 min and centrifuged at 13 000g for 15 min at 4 °C. Pellets were discarded and the supernatants were stored at −20 °C until further use. Protein concentration was determined using the Bradford assay (5 000 006, Bio-Rad). After that, 30 µg of protein from every sample were loaded into 10% acrylamide/bis-acrylamide gels and run in SDS-PAGE. Protein extracts from murine Mφ were loaded as well, as a positive control of NOS-2 expression. After that, proteins were transferred into PVDF membranes (1 704 157, Bio-Rad). The membranes were then blocked using 5% nonfat milk, washed with PBS, and incubated overnight with NOS-2 antibody (sc-7271, Santa Cruz) or β-actin antibody (A-5441, Sigma) as a loading control. Blots were developed using the ECL protocol and immunodetection was performed in a FUSION Solo 6S (Vilber).

Nitric Oxide Production Determination: For the in vitro experiments, nitric oxide synthesis was determined indirectly by evaluating nitrite production. Macrophage supernatant nitrite was quantified by the Griess assay. Briefly, after the previously described cell stimulation, supernatants from either human or murine Mφ were obtained. These supernatants were then centrifuged at 2 000g for 10 min at RT to eliminate residual cells. After that, the supernatants were placed in triplicate in a 96-well plate and Griess reagent (G4410, Sigma) was added at a final concentration of 20 mg mL^{−1} and incubated at RT for 15 min. Optical density was quantified in a spectrophotometer at 540 nm. Sodium nitrite was used as a reference standard for the analysis.

The generation of nitric oxide by DETA-NONATE was determined using a NO-sensitive electrode (ISO-NOP; World Precision Instruments Inc.) at 37 °C in constant stirring. The obtained values of intensity of current were interpolated with a standard curve elaborated with known concentrations of NO obtained from the decomposition of NaNO₂.

RNA Isolation and Analysis: RNA was extracted from hMφ using Tri Reagent solution (AM9738, Thermo Fisher), following the manufacturer's instructions. RNA quantification was measured in a NanoDrop 2000 (ThermoFisher). Then, 250 ng RNA was taken and reverse-transcribed into cDNA using the High Capacity cDNA Reverse Transcription kit (4 368 813, Applied Biosystems). After that, PCR was performed using 2.5 ng cDNA with Power SYBR Green PCR Master Mix (4 367 659, Applied Biosystems) and 250 nm of the corresponding primers (Table S1, Supporting Information) in a 7900HT Fast Real-Time PCR system (Applied Biosystems). The obtained CT measurements were analyzed following the 2^{−ΔΔCt} method using RPLP0 as a reference gene.

RNA Integrity Determination: RNA integrity was determined as a means of standardization of RNA quality. RNA was loaded in a micro-fabricated chip and separated by electrophoresis. After that, RNA was analyzed by fluorescence detection. The RNA was then assessed using the RNA Integrity Number (RIN) algorithm, which determines the quality of RNA depending on the shape of the curves obtained in the electropherogram. This algorithm classifies RNA quality on a scale from 1 to 10, where 1 was a completely degraded RNA and 10 is the intact RNA with no degradation. RNA samples that were above 7 were classified as qualified and were used for the RT-qPCR and RNAseq experiments, while RNA samples below 7 were not used.

RNAseq Experiments and Analysis: After cell treatment, RNA was isolated as previously described. The RNAseq procedure was realized by BGI as previously described.^[90] Briefly, to determine if the transcript was from a sense or antisense strand and its limits and number of copies, the Strand-Specific Transcriptome Library Construction Protocol (DNB-SEQ) was used. This library was completed by enriching mRNA from total RNA using oligo(dT)-attached magnetic beads. Then, mRNA molecules were broken into smaller fragments and the corresponding primers were added to synthesize the First Strand cDNA. For the Second Strand cDNA synthesis, dTTP was changed to dUTP, and the output was isolated using magnetic beads. The double-stranded cDNA end repair was achieved by specific enzymes and A nucleotides were added to the 3'-end during the PCR. A linker connection reaction system was used for adapter ligation, and the output was again purified using magnetic beads. The qual-

ity of the generated library was assessed in an Agilent Technologies 2100 bioanalyzer. The single-stranded DNA was circularized with the help of a splint oligo, generating single-stranded circular DNA fragments. To generate DNA Nanoballs (DNB), Rolling Circle Amplification (RCA) was performed, yielding a single-stranded DNA formed by multiple repetitions of the same sequence. DNBS are then loaded into a patterned nanarray. Finally, sequencing is achieved by combinatorial Probe Anchor Synthesis (cPAS), where dNTPs are incorporated, emitting a different fluorescent signal depending on which base they have incorporated.

Gene Expression Analysis: RNA sequencing was carried out in the DNBseq platform (Eukaryotic Strand Specific Transcriptome Resequencing product) applying its software to build the library (BGI; <https://www.bgi.com/global/home>). On average, 50.9 m clean reads were generated. Data quality Q20 parameter = 97.08%. Gene expression levels were calculated by the RSEM software package,^[97] Differential gene expression was filtered by DESeq2 algorithms (R-package) the parameters that were used to identify a gene as a DEG were the following: log₂FC ≥ |1| and p < 0.05. Ggplot2 package was used to elaborate plots and Genesis software,^[98] was the bioinformatic tool that allowed clustering and heatmap representation (<http://genome.tugraz.at/genesisclient/>). DEG enrichment sets were determined by ENRICH,^[99–101] (<http://amp.pharm.mssm.edu/Enrichr/>), and statistical significance was calculated by a Benjamini-Hochberg test. To perform the gene set enrichment analysis (GSEA) (<http://software.broadinstitute.org/gsea/index.jsp>;^[100]) broad Institute Data Base and NCBI Database were used (<https://www.ncbi.nlm.nih.gov/gds>). Functional annotation was conducted by consulting several databases: pathfinder,^[102] KEGG (<https://www.genome.jp/kegg>). The analysis was performed using the statistical computing environment R (4.1.1) in conjunction with the following packages: ComplexHeatmap (2.8.0),^[103] EnhancedVolcano (1.10.0),^[104] (<https://github.com/kevinblighe/EnhancedVolcano>) ggplot2 (3.3.5) to create volcano plots, heatmaps, and bubble charts; dplyr (1.0.7) to enable the dataset aggregation and analysis; VennDiagram (1.6.20) to create Venn diagrams graphic; and pathfindR (1.6.2) to perform enrichment analyses that identify active protein-protein interactions networks, identifying clusters of enriched terms and distinguish representative terms in each cluster. Package R was used for the statistical analysis of this section. GEO Submission (GSE236294; NCBI tracking system #24 115 068).

Construction of Condition-Specific GSMMs: The generic human Genome-Scale Metabolic Model (GSMM) Recon3D,^[56] was used as a template for reconstructing the GSMMs of hMφ under various conditions, including control conditions and different treatments (CK, DETA-NO, and DETA-NO+CK treatments). Computational analyses were performed using COBRAPy toolbox in python,^[105–107] Recon3D, which offers a comprehensive mathematical representation of known metabolic reactions for Homo sapiens in a cell- and tissue-agnostic manner, served as the foundation for our models. Recon3D was integrated with transcriptomics data, respiration data, and medium constraints (specifically, RPMI and 2% FBS) to establish the base model for condition-specific GSMMs. To mimic the metabolic, energetic, and reductive demands of hMφ, the macrophage biomass reaction was incorporated as described in reference,^[108] In addition, to build condition-specific GSMMs, enzymes with fragments per kb of exon per million mapped fragments (FPKM) under 1 were removed provided that their removal still enabled the models to produce 10% of optimal biomass.

Modulation of Metabolic Flux Distribution Using GIM3E: The GIM3E algorithm,^[58] was applied to compute a flux distribution for various conditions, including control, CK, DETA-NO, and DETA-NO plus CK treatments. This algorithm involves flux minimization weighted by gene expression, subject to achieving 10% of the optimal biomass production. GIM3E applies gene expression data to assign weights to each reaction, setting the reaction's minimization rate for subsequent flux calculations. The lower the expression levels the higher the minimization weight, ensuring a reduced flux value for the less expressed reactions. Thus, transcriptomics data are used to develop penalties (minimization weights) to reduce the use of reactions with lower evidence for expression. For each reaction, the associated weight (w_i) is computed from Equation (1) in which I_i indicates the log₂ intensity associated for gene i and $I_{i_{max}}$ indicates the maximum

threshold. I_{max} was calculated as the greatest value of all I_i . GIM3E was applied with the following restrictions:

$$\begin{aligned} & \text{Minimize } \sum w_i |v_i| \\ & w_i = \max(I_{max} - I_i) \\ & Sv = 0 \\ & LB_i \leq v_i \leq UB_i \\ & v_{obj} \geq f v_{obj}^{FBA} \end{aligned} \quad (1)$$

where S is the stoichiometric matrix and all reversible reactions have been split in irreversible format, v is the vector of reaction fluxes, LB_{i-i} and UB_i are the lower and upper bounds for flux I , v_{obj} is the objective function that should close to the optimum flux of an FBA calculation. Here, f is set to 0.99. Thus, flux variability analysis,^[56,106] is used to identify the solution space within 99% of the GIM3E optimal solution. Finally, the resulting solution space is sampled using the Artificially Centered hit-and-run (ACHR) algorithm COBRAPy,^[105,107] A total of 1 000 samples are generated with a thinning parameter (frequency of saved solutions) set at 100. From the output of the sampling, the mean and the standard deviation of all fluxes are obtained.

Subsequently, GIM3E algorithm and flux variability analysis were applied to compute the flux distribution for all conditions, including control, CK, DETA-NO, and DETA-NO plus CK treatments. To quantify itaconate (itacon_m) production, we first replaced the mitochondrial aconitase (ACO2) reaction, ACONtm (cit_m (citrate) \rightleftharpoons icit_m (isocitrate)), by the two intermediary reactions (r0317: cit_m \rightleftharpoons HC00342_m + h2o_m and r0426: icit_m \rightleftharpoons HC00342_m + h2o_m), leading to the formation of the intermediate metabolite cis-aconitate (HC00342_m). Second, the reaction of formation of itaconate from cis-aconitate catalyzed by aconitate decarboxylase 1 (ACOD1), GeneID 730 249 was implemented, (MAR13087 HC00342_m + h_m \rightarrow co2_m + itacon_m). Thus, in the model cis-aconitate could be transformed reversibly into citrate and isocitrate, and irreversibly to itaconate. Since cis-aconitate is formed from isocitrate, the reactions of cis-aconitate to citrate and cis-aconitate to itaconate were associated with a flux that depends on the relative gene expression. Thus, simulations were assigned to account for a minimum flux to form itaconate ($LB_{Itaconate}$), which depends on the differential gene expression of reactions associated with the formation of both itaconate and citrate from cis-aconitate. This process was fine-tuned to ensure the itaconate/citrate flux ratio matched the itaconate/citrate log2 ratio of gene expression. The inhibitory effect of NO on cytochrome c oxidase and aconitase,^[20] was introduced by knocking out genes with GeneIDs 4512, 4513, and 4514 (corresponding to cytochrome c oxidase I, II, and III, respectively), and r0317 and r0426 reactions.

For experimentally measured fluxes of glucose and lactate, the simulation minimizes the difference between simulated and measured values in each condition. As detailed in the following section, to validate the metabolic flux maps derived from each treatment, flux map distributions were computed using the qMTA algorithm,^[57] with the fluxes of the control serving as a reference.

Modulation of Metabolic Flux Distribution Using qMTA: The quadratic Metabolic Transformation Algorithm (qMTA),^[57] was applied to simulate the metabolic switch between two metabolic states (control (or reference) and treatment) by minimizing the following expression of three terms that depend on differential gene expression, reaction fluxes, and experimentally measured fluxes.

$$\begin{aligned} & \min \sum_{m \in DExp} \left(W_m \sum_{i \in R_m} \left(\frac{v_i^{ref} \cdot FC_m - v_i^{MTA}}{v_i^{ref} (FC_m - 1)} \right)^2 \right) + \sum_{i \in Ru} \frac{(v_i^{ref} - v_i^{MTA})^2}{v_i^{ref}} \\ & + \sum_{j \in Rexp} \frac{(E_j - v_j^{MTA})^2}{\sigma_j} \end{aligned} \quad (2)$$

$$s \cdot v^{MTA} = 0 \quad (3)$$

$$LB_i \leq v_i \leq UB_i \quad (4)$$

where W_{genes} , $W_{reactions}$, and W_{kpc} are the weights of the three terms using the values of 0.1, 0.1, and 1, respectively. $DExp$ is a set of differentially expressed genes between the conditions, W_m is the weight given to gene m , R_m is a set of reactions associated with gene m (defined using Recon3D's gene reactions rules); v_i^{ref} and v_i^{MTA} are control/reference and treatment fluxes, respectively; FC_m is the fold change of gene m expression relative to control; Ru is the set of reactions not associated with differentially expressed genes or experimental measures; $Rexp$ is the set of fluxes measured experimentally; E_j is the mean experimental flux measured for reaction j ; σ_j is the experimental standard deviation of the measured flux for reaction j ; s is the stoichiometric matrix of the condition-specific model; lb and ub indicate the flux lower and upper bounds, respectively.

The optimization minimizes the difference between the simulated flux values and target flux considering the gene expression fold change for each differentially expressed gene mapped to any given reaction. For reactions that are not mapped to differentially expressed genes, the flux variation is minimized instead. Both terms of the optimization are scaled by the reference flux distribution to prevent a bias of reactions with high referenced flux. Again, for experimentally measured fluxes the difference between simulated and measured values is minimized and weighted by the experimental standard deviations. Each differentially expressed gene is given a weight (W_m) calculated from (Equation (5)).

$$W_m = \log_{10}(p_{th}) - \log_{10}(p_m) \quad (5)$$

where p_{th} is the p-value threshold (fixed to 0.25 in this study), which determines whether a gene is differentially expressed and p_m is the p-adjusted values associated with a given gene expression fold change relative to the control. The results obtained through this analysis were compared with those obtained using the GIM3E method, ensuring consistency between the outcomes generated by both algorithms. The same treatment for the production of itaconate was performed as in the case of GIM3E method.

Experimental Data Used for In-Silico Simulations: The model was trained with transcriptomic data from hMφ obtained from 4 conditions. being 10⁷ hMφ cultured per sample (RPMT + 2% FBS). Additionally, respiration parameters (OCR, basal respiration, and ATP production) from hMφ were used to constrain the model in conditions using DETA-NO.

Statistical Analysis: Values in graphs correspond to mean \pm SD. The statistical significance of differences between the means was determined with GraphPad Prism 9.0.0. (GraphPad Software) using a one-way analysis of variance (ANOVA) followed by Bonferroni post hoc test or Student's t-test, as appropriate. A P-value <0.05 was considered to be significant. Pathway graphs were generated by aggregating the contributions of fluxes associated with all reactions that are constituents of each respective pathway. The uncertainty related to each path was determined from the standard deviations of contributing reactions obtained from the ACHR sampling procedure.

Supporting Information

Supporting Information is available from the Wiley Online Library or from the author.

Acknowledgements

The authors thank the services of flow cytometry and genomics from the IIBM for technical support. The authors thank Susana Cadenas from Centro de Biología Molecular "Severo Ochoa" for her help with the NO-sensitive electrode measurements; Santiago Lamas and Carlos Rey,

from the same centre, for their help with the Seahorse measurements; and Carles Foguet from Cambridge University, UK for his technical advice in bioinformatics. We acknowledge support of the publication fee by the CSIC Open Access Publication Support Initiative (URICI). **Funding sources.** This work has been supported by: PID2020-113238RB-I00 and PID2020-115051RB-I00 from MICIN/AEI 13039/501100011033, and Centro de Investigación Biomédica en Red en Enfermedades Cardiovasculares (CB16/11/00222) y en Enfermedades Hepáticas y Digestivas (CB17/04/00023) from the Instituto de Salud Carlos III (co-financed by the European Development Regional Fund “A Way to Achieve Europe”, by the “European Union” and by the “European Union NextGeneration EU/PRTR”); Comunidad de Madrid, Programa Biociencias (S2022-BMD-7223); from AGAUR (2021 SGR 00350 and 2020PANDE00048) of Generalitat de Catalunya (MC); and Spanish Structures of Excellence María de Maeztu program (CEX2021-001202-M).

Conflict of Interest

The authors declare no conflict of interest.

Author Contributions

S.S.-G. and A.P.-R. contributed equally to the work, designed the study and performed experiments, analyzed data, prepared the figures, and revised the manuscript. A.P.-R., C.A.-L, and S.M. performed specific metabolic assays and contributed to data analysis. A.C. and J.V.R. analyzed and elaborated the transcriptomic data. S.M., M.F., S.M., N.A., and M.C. developed and applied the GSMM and analyzed the flux modeling results. S.M. and N.A. prepared the metabolic flux analysis figures. S.S.-G., A.P.-R., and P.P. provided intellectual input and improvements, discussed results, and revised the manuscript. All authors provided intellectual input and revised the manuscript. S.S.-G., S.M. M.C., and L.B. analyzed and discussed the results, wrote the paper, provided funding and intellectual input, and organized the information.

Data Availability Statement

The data that support the findings of this study are openly available in NCBI at <https://www.ncbi.nlm.nih.gov/doi/10.1002/adhm.202401688>, reference number 24115068. These data were derived from the following resources available in the public domain: [Resource 1], <https://www.github.com/kevinblighe/EnhancedVolcano>; <https://www.github.com/kevinblighe/EnhancedVolcano>, <https://www.github.com/kevinblighe/EnhancedVolcano>.

Keywords

COVID-19, immunometabolism, macrophage, nitric oxide, ROS

Received: May 25, 2024

Revised: October 4, 2024

Published online: November 6, 2024

- [1] B. Hu, H. Guo, P. Zhou, Z.-L. Shi, *Nat. Rev. Microbiol.* **2021**, *19*, 141.
- [2] Q. Zhang, R. Xiang, S. Huo, Y. Zhou, S. Jiang, Q. Wang, F. Yu, *Signal Transduct. Target. Ther.* **2021**, *6*, 233.
- [3] P. Xie, W. Ma, H. Tang, D. Liu, *Front. Public. Heal.* **2020**, *8*, 189.
- [4] R. Q. Cron, G. Goyal, W. W. Chatham, *Annu. Rev. Med.* **2023**, *74*, 321.
- [5] D. C. Fajgenbaum, C. H. June, *N. Engl. J. Med.* **2020**, *383*, 2255.
- [6] K. Jarnagin, O. Alvarez, S. Shrestha, D. R. Webb, *Biochem. Pharmacol.* **2021**, *188*, 114543.

- [7] M. D. Johansen, A. Irving, X. Montagutelli, M. D. Tate, I. Rudloff, M. F. Nold, N. G. Hansbro, R. Y. Kim, C. Donovan, G. Liu, A. Faiz, K. R. Short, J. G. Lyons, G. W. McCaughan, M. D. Gorrell, A. Cole, C. Moreno, D. Couteur, D. Hesselton, J. Triccas, G. G. Neely, J. R. Gamble, S. J. Simpson, B. M. Saunders, B. G. Oliver, W. J. Britton, P. A. Wark, C. A. Nold-Petry, P. M. Hansbro, *Mucosal Immunol.* **2020**, *13*, 877.
- [8] D. Wrapp, N. Wang, K. S. Corbett, J. A. Goldsmith, C.-L. Hsieh, O. Abiona, B. S. Graham, J. S. McLellan, *Science* **2020**, *367*, 1260.
- [9] L. J. Ignarro, *Br. J. Pharmacol.* **2020**, *16*, 3848.
- [10] N. C. Adusumilli, D. Zhang, J. M. Friedman, A. J. Friedman, *Nitric Oxide* **2020**, *103*, 4.
- [11] M. Ferrari, A. Protti, *eBioMedicine* **2022**, *77*, 103925.
- [12] A. Nikolaidis, R. Kramer, S. Ostojic, *Med. Sci.* **2021**, *10*, 3.
- [13] R. Rajendran, A. Chathambath, A. G. Al-Sehemi, M. Pannipara, M. K. Unnikrishnan, L. Aleya, R. P. Raghavan, B. Mathew, *Environ. Sci. Pollut. Res.* **2022**, *29*, 38657.
- [14] R. A. Alvarez, L. Berra, M. T. Gladwin, *Am. J. Respir. Crit. Care Med.* **2020**, *202*, 16.
- [15] K. Willmann, L. F. Moita, *Cell Metab.* **2024**, *36*, 927.
- [16] Y. Liu, R. Xu, H. Gu, E. Zhang, J. Qu, W. Cao, X. Huang, H. Yan, J. He, Z. Cai, *Biomark. Res.* **2021**, *9*, 1.
- [17] J. C. Rodriguez-Prados, P. G. Traves, J. Cuenca, D. Rico, J. Aragones, P. Martin-Sanz, M. Cascante, L. Bosca, *J. Immunol.* **2010**, *185*, 605.
- [18] A. Hooftman, L. A. J. O'Neill, *Trends Immunol.* **2019**, *40*, 687.
- [19] A. Tawakol, P. Singh, M. Mojena, M. Pimentel-Santillana, H. Emami, M. MacNabb, J. H. F. Rudd, J. Narula, J. A. Enriquez, P. G. Través, M. Fernández-Velasco, R. Bartrons, P. Martín-Sanz, Z. A. Fayad, A. Tejedor, L. Boscá, *Arterioscler. Thromb. Vasc. Biol.* **2015**, *35*, 1463.
- [20] E. M. Palmieri, M. Gonzalez-Cotto, W. A. Baseler, L. C. Davies, B. Ghesquière, N. Maio, C. M. Rice, T. A. Rouault, T. Cassel, R. M. Higashi, A. N. Lane, T. W.-M. Fan, D. A. Wink, D. W. McVicar, *Nat. Commun.* **2020**, *11*, 698.
- [21] G. Pappas, M. L. Wilkinson, A. J. Gow, *Nitric Oxide* **2023**, *131*, 8.
- [22] A. C. Codo, G. G. Davanzo, L. D. B. Monteiro, G. F. de Souza, S. P. Muraro, J. V. Virgilio-da-Silva, J. S. Prodonoff, V. C. Carregari, C. A. O. de Biagi Junior, F. Crunfli, J. L. Jimenez Restrepo, P. H. Vendramini, G. Reis-de-Oliveira, K. Bispo dos Santos, D. A. Toledo-Teixeira, P. L. Parise, M. C. Martini, R. E. Marques, H. R. Carmo, A. Borin, L. D. Coimbra, V. O. Boldrini, N. S. Brunetti, A. S. Vieira, E. Mansour, R. G. Ulaf, A. F. Bernardes, T. A. Nunes, L. C. Ribeiro, A. C. Palma, et al., *Cell Metab.* **2020**, *32*, 437.
- [23] N. Xiao, M. Nie, H. Pang, B. Wang, J. Hu, X. Meng, K.e Li, X. Ran, Q. Long, H. Deng, N.a Chen, S. Li, N. Tang, A. Huang, Z. Hu, *Nat. Commun.* **2021**, *12*, 1618.
- [24] N. Takeda, E. L. O'Dea, A. Doedens, J. Kim, A. Weidemann, C. Stockmann, M. Asagiri, M. C. Simon, A. Hoffmann, R. S. Johnson, *Genes Dev.* **2010**, *24*, 491.
- [25] U. R. Mbonye, C. Yuan, C. E. Harris, R. S. Sidhu, I. Song, T. Arakawa, W. L. Smith, *J. Biol. Chem.* **2008**, *283*, 8611.
- [26] D. Rico, J. M. Vaquerizas, H. Dopazo, L. Boscá, *BMC Genomics* **2007**, *8*, 271.
- [27] L. Bosca, S. Hortelano, L. Boscá, S. Hortelano, L. Bosca, S. Hortelano, *Cell Signal* **1999**, *11*, 239.
- [28] W. Fang, J. Jiang, L. Su, T. Shu, H. Liu, S. Lai, R. A. Ghiladi, J. Wang, *Biol. Med.* **2021**, *163*, 153.
- [29] A. Povo-Retana, R. Landauro-Vera, M. Fariñas, S. Sánchez-García, C. Alvarez-Lucena, S. Marin, M. Cascante, L. Boscá, *Biochem. Soc. Trans.* **2023**, *51*, 1429.
- [30] M. E. de Vera, R. A. Shapiro, A. K. Nussler, J. S. Mudgett, R. L. Simmons, S. M. Morris, T. R. Billiar, D. A. Geller, *Proc. Natl. Acad. Sci. USA* **1996**, *93*, 1054.
- [31] D. Ben-Avraham, R. H. Muzumdar, G. Atzmon, *EpigenomicsEpigenomics* **2012**, *4*, 503.

- [32] G. C. Chan, J. E. Fish, I. A. Mawji, D. D. Leung, A. C. Rachlis, P. A. Marsden, *J. Immunol.* **2005**, *175*, 3846.
- [33] W. Xu, S. Humphries, M. Tomita, T. Okuyama, M. Matsuki, D. Burgner, D. Kwiatkowski, L. Liu, I. G. Charles, *Nitric Oxide* **2000**, *4*, 379.
- [34] Z. Guo, L. Shao, L. Zheng, Q. Du, P. Li, B. John, D. A. Geller, *Proc. Natl. Acad. Sci.* **2012**, *109*, 5826.
- [35] S. B. Wiegand, B. Safaee Fakhr, R. W. Carroll, W. M. Zapol, R. M. Kacmarek, L. Berra, *Crit. Care Explor.* **2020**, *2*, e0277.
- [36] J. Kobayashi, I. Murata, *Ann. Intensive Care* **2020**, *10*, 61.
- [37] A. M. Genaro, S. Hortelano, A. Alvarez, C. Martínez-A, L. Bosca, *J. Clin. Invest.* **1995**, *95*, 1884.
- [38] L. Bosca, M. Zeini, P. Traves, S. Hortelano, *Toxicology* **2005**, *208*, 249.
- [39] A. Ghosh, B. Joseph, S. Anil, *Cureus* **2022**, *14*, e23852.
- [40] N. S. Bryan, J. Molnar, J. Somberg, *Am. J. Med.* **2023**, *136*, 1035.
- [41] V. Carlini, D. M. Noonan, E. Abdalalem, D. Goletti, C. Sansone, L. Calabrone, A. Albini, *Front. Immunol.* **2023**, *14*, 1161067.
- [42] D. M. Del Valle, S. Kim-Schulze, H.-H. Huang, N. D. Beckmann, S. Nirenberg, B. Wang, Y. Lavin, T. H. Swartz, D. Madduri, A. Stock, T. U. Marron, H. Xie, M. Patel, K. Tuballes, O. Van Oekelen, A. Rahman, P. Kovatch, J. A. Aberg, E. Schadt, S. Jagannath, M. Mazumdar, A. W. Charney, A. Firpo-Betancourt, D. R. Mendu, J. Jhang, D. Reich, K. Sigel, C. Cordon-Cardo, M. Feldmann, S. Parekh, et al., *Nat. Med.* **2020**, *26*, 1636.
- [43] J. Wang, M. Jiang, X. Chen, L. J. Montaner, *J. Leukoc. Biol.* **2020**, *108*, 17.
- [44] H. Akbari, R. Tabrizi, K. B. Lankarani, H. Aria, S. Vakili, F. Asadian, S. Noroozi, P. Keshavarz, S. Faramarz, *Life Sci.* **2020**, *258*, 118167.
- [45] S. Hortelano, A. M. Alvarez, L. Bosca, *FASEB J.* **1999**, *13*, 2311.
- [46] F. Antunes, A. Boveris, E. Cadenas, *Proc. Natl. Acad. Sci.* **2004**, *101*, 16774.
- [47] G. Krzak, C. M. Willis, J. A. Smith, S. Pluchino, L. Peruzzotti-Jametti, *Trends Immunol.* **2021**, *42*, 45.
- [48] P. Chen, H. Zuo, H. Xiong, M. J. Kolar, Q. Chu, A. Saghatelian, D. J. Siegwart, Y. Wan, *Proc. Natl. Acad. Sci.* **2017**, *114*, 580.
- [49] C.-Y. Lai, P.-C. Tseng, C.-L. Chen, R. D. Satria, Y.-T. Wang, C.-F. Lin, *J. Inflamm. Res.* **2021**, *14*, 5241.
- [50] E. Clementi, G. C. Brown, M. Feelisch, S. Moncada, *Proc. Natl. Acad. Sci.* **1998**, *95*, 7631.
- [51] Y. Gartshteyn, A. D. Askanase, A. Mor, *Front. Immunol.* **2021**, *12*, 654839.
- [52] B. Blasco-Moreno, L. de Campos-Mata, R. Böttcher, J. García-Martínez, J. Jungfleisch, D. D. Nedialkova, S. Chattopadhyay, M.-E. Gas, B. Oliva, J. E. Pérez-Ortín, S. A. Leidel, M. Choder, J. Díez, *Nat. Commun.* **2019**, *10*, 1298.
- [53] A. Zaghlool, J. Halvardson, J. J. Zhao, M. Etemadikhah, A. Kalushkova, K. Konska, H. Jernberg-Wiklund, A. Thuresson, L. Feuk, *Hum. Mutat.* **2016**, *37*, 964.
- [54] W. Chen, T. Jiang, H. Wang, S. Tao, A. Lau, D. Fang, D. D. Zhang, *Antioxid. Redox Signal.* **2012**, *17*, 1670.
- [55] F. D'Acquisto, F. de Cristofaro, M. C. Maiuri, G. Tajana, R. Carnuccio, *Cell Death Differ.* **2001**, *8*, 144.
- [56] E. Brunk, S. Sahoo, D. C. Zielinski, A. Altunkaya, A. Dräger, N. Mih, F. Gatto, A. Nilsson, G. A. Preciat Gonzalez, M. K. Aurich, A. Prlic, A. Sastry, A. D. Danielsdottir, A. Heinken, A. Noronha, P. W. Rose, S. K. Burley, R. M. T. Fleming, J. Nielsen, I. Thiele, B. O. Palsson, *Nat. Biotechnol.* **2018**, *36*, 272.
- [57] C. Foguet, Y. Xu, S. C. Ritchie, S. A. Lambert, E. Persyn, A. P. Nath, E. E. Davenport, D. J. Roberts, D. S. Paul, E. Di Angelantonio, J. Danesh, A. S. Butterworth, C. Yau, M. Inouye, *Nat. Commun.* **2022**, *13*, 7356.
- [58] B. J. Schmidt, A. Ebrahim, T. O. Metz, J. N. Adkins, B. Ø. Palsson, D. R. Hyduke, *Bioinformatics* **2013**, *29*, 2900.
- [59] M. P. Murphy, L. A. J. O'Neill, *Cell* **2018**, *174*, 780.
- [60] D. G. Ryan, L. A. J. O'Neill, *Annu. Rev. Immunol.* **2020**, *38*, 289.
- [61] S. S. Gross, M. S. Wolin, *Annu. Rev. Physiol.* **1995**, *57*, 737.
- [62] L. Liu, J. S. Stampler, *Cell Death Differ.* **1999**, *6*, 937.
- [63] J. MacMicking, Q. Xie, C. Nathan, *Annu. Rev. Immunol.* **1997**, *15*, 323.
- [64] J. E. Albina, *J. Leukoc. Biol.* **1995**, *58*, 643.
- [65] M. Schneemann, G. Schoedon, S. Hofer, N. Blau, L. Guerrero, A. Schaffner, *J. Infect. Dis.* **1993**, *167*, 1358.
- [66] A. R. Amin, M. Attur, P. Vyas, J. Leszczynska-Piziak, D. Levartovsky, J. Rediske, R. M. Clancy, K. A. Vora, S. B. Abramson, *J. Inflamm.* **1995**, *47*, 190.
- [67] K. T. Cheung, D. M.-Y. Sze, K. H. Chan, P. H.-M. Leung, *Immunobiology* **2018**, *223*, 356.
- [68] Y. Yang, H. Wang, M. Kouadir, H. Song, F. Shi, *Cell Death Dis.* **2019**, *10*, 128.
- [69] B. K. Gajjela, M.-M. Zhou, *Drug Discov. Today* **2022**, *27*, 390.
- [70] S. Hortelano, P. G. Través, M. Zeini, A. M. Alvarez, L. Bosca, *J. Immunol.* **2003**, *171*, 6059.
- [71] J. D. Erusalimsky, S. Moncada, *Arterioscler. Thromb. Vasc. Biol.* **2007**, *27*, 2524.
- [72] S. Bartesaghi, R. Radi, *Redox Biol.* **2018**, *14*, 618.
- [73] G. L. Semenza, *Curr. Opin. Cell Biol.* **2001**, *13*, 167.
- [74] H. Islam, T. C. Chamberlain, A. L. Mui, J. P. Little, *Front. Immunol.* **2021**, *12*, 67708.
- [75] J. Schaale, J. Brandenburg, A. Kispert, M. Leitges, S. Ehlers, N. Reiling, *J. Immunol.* **2013**, *191*, 5182.
- [76] S. Pagie, N. Gérard, B. Charreau, *Cell Commun. Signal.* **2018**, *16*, 4.
- [77] E. Y. Chung, J. Liu, Y. Homma, Y. Zhang, A. Brendolan, M. Saggese, J. Han, R. Silverstein, L. Selleri, X. Ma, *Immunity* **2007**, *27*, 952.
- [78] X.-X. Chen, L. Tang, Y.-M. Fu, Y. Wang, Z.-H. Han, J.-G. Meng, *Int. J. Mol. Med.* **2017**, *40*, 1921.
- [79] X. Zhao, X. Zhou, H. Sun, H. Shi, Y. Song, Q. Wang, G. Zhang, D. Xu, *Front. Immunol.* **2022**, *13*, 1001526.
- [80] K. Abbas, J. Breton, A. G. Planson, C. Bouton, J. Bignon, C. Seguin, S. Riquier, M. B. Toledano, J. C. Drapier, *Free Radic Biol Med.* **2011**, *51*, 107.
- [81] S. Fiorucci, A. Mencarelli, E. Distrutti, M. Baldoni, P. del Soldato, A. Morelli, *J. Immunol.* **2004**, *173*, 874.
- [82] P. R. Gardner, G. Costantino, C. Szabó, A. L. Salzman, *J. Biol. Chem.* **1997**, *272*, 25071.
- [83] C. E. Cooper, *Biochim. Biophys. Acta – Bioenerg.* **1999**, *1411*, 290.
- [84] X. Zhu, D. Long, M. Zabalawi, B. Ingram, B. K. Yoza, P. W. Stacpoole, C. E. McCall, *J. Leukoc. Biol.* **2020**, *107*, 467.
- [85] A. Heinz, Y. Nonnenmacher, A. Henne, M.-A. Khalil, K. Bejkollari, C. Dostert, S. Hosseini, O. Goldmann, W. He, R. Palorini, C. Verschuere, M. Korte, F. Chiaradonna, E. Medina, D. Brenner, K. Hiller, *Biochim. Biophys. Acta – Mol. Basis Dis.* **2022**, *1868*, 166530.
- [86] L. A. J. O'Neill, M. N. Artyomov, *Nat. Rev. Immunol.* **2019**, *19*, 273.
- [87] H. Zhang, C. Zhang, W. Hua, J. Chen, *Med. Gas Res.* **2024**, *14*, 39.
- [88] R. Di Fenza, N. S. Shetty, S. Gianni, V. Parcha, V. Giammatteo, B. Safaee Fakhr, D. Tornberg, O. Wall, P. Harbut, P. S. Lai, J. Z. Li, S. Paganoni, S. Cenci, A. L. Mueller, T. T. Houle, O. Akeju, E. A. Bittner, S. Bose, L. K. Scott, R. W. Carroll, F. Ichinose, M. Hedenstierna, P. Arora, L. Berra, C. C. A. Morais, L. E. Gibson, T. Ikeda, E. Marutani, Y. Miyazaki, A. Fischbach, et al., *Am. J. Respir. Crit. Care Med.* **2023**, *208*, 1293.
- [89] D. Sang, K. Lin, Y. Yang, G. Ran, B. Li, C. Chen, Q. Li, Y. Ma, L. Lu, X.-Y. Cui, Z. Liu, S.-Q. Lv, M. Luo, Q. Liu, Y. Li, E. E. Zhang, *Cell* **2023**, *186*, 5500.
- [90] A. Povo-Retana, M. Fariñas, R. Landauro-Vera, M. Mojena, C. Alvarez-Lucena, M. A. Fernández-Moreno, A. Castrillo, J. V. de la Rosa Medina, S. Sánchez-García, C. Foguet, F. Mas, S. Marin, M. Cascante, L. Bosca, *Front. Immunol.* **2023**, *14*, 1211068.

- [91] R. I. Jaén, M. Fernández-Velasco, V. Terrón, S. Sánchez-García, C. Zaragoza, N. Canales-Bueno, A. Val-Blasco, M. T. Vallejo-Cremades, L. Boscá, P. Prieto, *FASEB J.* **2020**, *34*, 10531.
- [92] A. Castrillo, M. Mojena, S. Hortelano, L. Boscá, *J. Biol. Chem.* **2001**, *276*, 34082.
- [93] T. Ishimoto, O. Nagano, T. Yae, M. Tamada, T. Motohara, H. Oshima, M. Oshima, T. Ikeda, R. Asaba, H. Yagi, T. Masuko, T. Shimizu, T. Ishikawa, K. Kai, E. Takahashi, Y. Imamura, Y. Baba, M. Ohmura, M. Suematsu, H. Baba, H. Saya, *Cancer Cell* **2011**, *19*, 387.
- [94] F. Kuang, J. Liu, D. Tang, R. Kang, *Front. Cell Dev. Biol.* **2020**, *8*, 969.
- [95] A. Povo-Retana, M. Mojena, A. Boscá, J. Pedrós, D. A. Peraza, C. Valenzuela, J. M. Laparra, F. Calle, L. Boscá, *Adv. Biol.* **2021**, *5*, e2100882.
- [96] S. Hortelano, M. L. García-Martín, S. Cerdán, A. Castrillo, A. M. Alvarez, L. Boscá, *Cell Death Differ.* **2001**, *8*, 1022.
- [97] I. Eguíluz-Gracia, H. H. L. Schultz, L. I. B. Sikkeland, E. Danilova, A. M. Holm, C. J. H. Pronk, W. W. Agace, M. Iversen, C. Andersen, F. L. Jahnsen, E. S. Baekkevold, *Thorax* **2016**, *71*, 1006.
- [98] M. Haniffa, F. Ginhoux, X.-N. Wang, V. Bigley, M. Abel, I. Dimmick, S. Bullock, M. Grisotto, T. Booth, P. Taub, C. Hilkens, M. Merad, M. Collin, *J. Exp. Med.* **2009**, *206*, 371.
- [99] Z. Bian, Y. Gong, T. Huang, C. Z. W. Lee, L. Bian, Z. Bai, H. Shi, Y. Zeng, C. Liu, J. He, J. Zhou, X. Li, Z. Li, Y. Ni, C. Ma, L. Cui, R. Zhang, J. K. Y. Chan, L. G. Ng, Y. Lan, F. Ginhoux, B. Liu, *Nature* **2020**, *582*, 571.
- [100] F. Ginhoux, M. Williams, *Immunity* **2016**, *44*, 439.
- [101] S. Müller, G. Kohanbash, S. J. Liu, B. Alvarado, D. Carrera, A. Bhaduri, P. B. Watchmaker, G. Yagnik, E. Di Lullo, M. Malatesta, N. M. Amankulor, A. R. Kriegstein, D. A. Lim, M. Aghi, H. Okada, A. Diaz, *Genome Biol.* **2017**, *18*, 234.
- [102] E. Ulgen, O. Ozisik, O. U. Sezerman, *Front. Genet.* **2019**, *10*, 858.
- [103] Z. Gu, R. Eils, M. Schlesner, *Bioinformatics* **2016**, *32*, 2847.
- [104] K. Blighe, S. Rana, M. Lewis, EnhancedVolcano: Publication-ready volcano plots with enhanced colouring and labeling. R package version **2024**, <https://github.com/kevinblighe/EnhancedVolcano>.
- [105] A. Ebrahim, J. A. Lerman, B. O. Palsson, D. R. Hyduke, *BMC Syst. Biol.* **2013**, *7*, 74.
- [106] S. Gudmundsson, I. Thiele, *BMC Bioinformatics* **2010**, *11*, 489.
- [107] L. Heirendt, S. Arreckx, T. Pfau, S. N. Mendoza, A. Richelle, A. Heinken, H. S. Haraldsdóttir, J. Wachowiak, S. M. Keating, V. Vlasov, S. Magnúsdóttir, C. Y. Ng, G. Preciat, A. Zagare, S. H. J. Chan, M. K. Aurich, C. M. Clancy, J. Modamio, J. T. Sauls, A. Noronha, A. Bordbar, B. Cousins, D. C. El Assal, L. V. Valcarcel, I. Apaolaza, S. Ghaderi, M. Ahoosh, M. Ben Guebila, A. Kostromins, N. Sompairac, et al., *Nat. Protoc.* **2019**, *14*, 639.
- [108] A. Bordbar, N. E. Lewis, J. Schellenberger, B. Ø. Palsson, N. Jamshidi, *Mol. Syst. Biol.* **2010**, *6*, 422.